SPRAY DRYING AND ATTRITION BEHAVIOR OF IRON CATALYSTS FOR

SLURRY PHASE FISCHER-TROPSCH SYNTHESIS

A Thesis

by

VÍCTOR HUGO CARRETO VÁZQUEZ

Submitted to the Office of Graduate Studies of
Texas A&M University
in partial fulfillment of the requirements for the degree of

MASTER OF SCIENCE

August 2003

Major Subject: Chemical Engineering

SPRAY DRYING AND ATTRITION BEHAVIOR OF IRON CATALYSTS FOR

SLURRY PHASE FISCHER-TROPSCH SYNTHESIS

A Thesis

by

VÍCTOR HUGO CARRETO VÁZQUEZ

Submitted to Texas A&M University
in partial fulfillment of the requirements
for the degree of

MASTER OF SCIENCE

Approved as to style and content by:

_____	_____
Dragomir B. Bukur	Aydin A. Akgerman
(Chair of Committee)	(Member)
_____	_____
John P. Wagner	Kenneth R. Hall
(Member)	(Head of Department)

August 2003

Major Subject: Chemical Engineering

ABSTRACT

Spray Drying and Attrition Behavior of Iron Catalysts for Slurry Phase Fischer-Tropsch
Synthesis. (August 2003)

Víctor Hugo Carreto Vázquez, B.S., E.S.I.Q.I.E. – I.P.N.

Chair of Advisory Committee: Dr. Dragomir B. Bukur

This thesis describes results of a study aimed at developing and evaluating attrition resistant iron catalysts prepared by spray drying technique. These catalysts are intended for Fischer-Tropsch (F-T) synthesis in a slurry bubble column reactor (SBCR). One of the major challenges associated with the use of SBCR for this purpose is the problem of catalyst/wax separation. If the catalyst particles break up into smaller ones during the F-T synthesis, these small particles (>5-10 μm in diameter) will cause problems with the catalyst/wax separation. Several research groups have worked on development of attrition resistant spray-dried iron catalysts, and methodology to measure and predict their attrition behavior. However, these attrition tests were not conducted under conditions representative of those encountered in a SBCR.

In this work, the attrition behavior of six spray-dried catalysts and two precipitated catalysts was evaluated under slurry reaction conditions in a stirred tank slurry reactor (STSR). Spray-dried catalysts used in this study were prepared at Texas A&M University (TAMU) and at Hampton University (HU), employing different preparation procedures and silica sources (potassium silicate, tetraethyl orthosilicate or colloidal silica). The attrition properties of F-T catalysts were determined by measuring particle size distribution (PSD) of catalysts before and after F-T synthesis in the STSR. This provides a direct measure of changes in particle size distribution in the STSR, and accounts for both physical and chemical attrition effects. Also, scanning electron microscopy (SEM) was used to investigate the mechanism of attrition - erosion vs.

fracture, and to obtain morphological characteristics of catalysts. Spray dried 100Fe/3Cu/5K/16SiO$_2$ catalyst (WCS3516-1), prepared from wet precursors using colloidal silica as the silica source, was the best in terms of its attrition strength. After 337 hours of F-T synthesis in the STSR, the reduction in the average particle size and generation of particles less than 10 μm in diameter were found to be very small. This indicates that both particle fracture and erosion were insignificant during testing in the STSR. All other catalysts, except one of the spray dried catalysts synthesized at Hampton University, also had a good attrition resistance and would be suitable for use in slurry reactors for F-T synthesis.

ACKNOWLEDGEMENTS

TABLE OF CONTENTS

LIST OF FIGURES

LIST OF TABLES

INTRODUCTION

Fischer-Tropsch (F-T) synthesis is a well-known process, which was discovered in Germany during the first half of the last century. This process was commercialized in Germany during the Second World War to provide an independent source of transportation liquid fuels from the conversion of synthesis gas into high-molecular weight hydrocarbons [1]. Synthesis gas ($CO + H_2$) was obtained from brown coal gasification, and the reaction was carried out in fixed bed reactors using supported cobalt catalysts.

F-T synthesis has been practiced on commercial scale at Sasol's plants in South Africa since mid 1950's. Originally, tubular fixed bed reactors (TFB) were used to produce primarily diesel fuel and hydrocarbon wax, whereas circulating fluidized bed (CFB) reactors were used for the production of gasoline and α-olefins [2]. Precipitated iron catalysts have been used in TFB reactors, whereas fused iron catalysts have been used in CFB reactors. Each of these two reactor types has a narrow range of operating conditions in relation to fresh feed composition and the temperature of the reaction. Both reactor types are not suitable for direct processing of synthesis gas with hydrogen to carbon monoxide (H_2/CO) molar feed ratio between 0.5 and 0.7, which is produced in advanced coal gasifiers.

In order to avoid some of the limitations of the TFB and CFB reactors, Sasol has continued to work on development of more effective reactors for F-T synthesis [3-6]. A new commercial scale conventional fluidized bed reactor and a slurry bubble column reactor (SBCR) have been constructed and placed on stream in 1990 and 1993, respectively [7]. These reactors are less expensive to construct, maintain and operate

---

This thesis follows the style and format of Applied Catalysis A: General.

than the TFB and CFB reactors. Some advantages of slurry processing and SBCRs are summarized below:

- SBCRs are cost-effective to operate, as well as, to construct and maintain.
- SBCRs are highly flexible, providing the ability to operate in either gasoline or wax mode of operation [5].
- SBCRs have the ability to more readily remove the heat generated during the reaction, which eliminates the localized hot spots. Because of the improved temperature control, yield losses to methane are reduced and catalyst deactivation due to coking is decreased [8].
- SBCRs offer higher conversion per pass and can utilize carbon monoxide-rich synthesis gas feed (H_2/CO ratio, 0.5-0.7) without requiring previous water-gas shift [9].

A commercial size (5 m in diameter, 22 m in height) slurry bubble column reactor was commissioned by Sasol in May 1993, and has been reported to operate successfully since that time [1,5].

Development of the appropriate catalysts for use in slurry reactors is an issue of essential importance for advancement of F-T technology. Catalyst particles in SBCRs are small (30-90 μm in diameter) and they are suspended in a slurry medium. During the reactor operation it is necessary to remove wax produced during F-T synthesis from the reactor, while keeping catalyst in the reactor. Catalyst/wax separation can be accomplished either by using internal separators (e.g. filters) which allow clean wax to pass through while keeping the catalyst inside the reactor, or by using external separators. In the latter case the slurry is removed from the reactor and separation is effected in an external separator, and the catalyst is returned back to the reactor. In this context, Sasol has also worked on development of catalysts with high mechanical strength or attrition resistance to avoid generation of small particles during the F-T synthesis. These small particles

(less than about 5 μm in diameter) are difficult to separate from the wax, regardless whether internal or external separators are employed. Jager and Espinoza [5] described in general terms the preparation of a catalyst for use in the slurry bubble column reactor, and stated that solid/wax separation was a major developmental challenge. The catalyst was spray dried to produce spherical particles. They claim that the formation of spherical particles in a spray drier is essential for maintaining their mechanical integrity during F-T synthesis. Figure 1 shows two scanning electron microscopy (SEM) images of spray-dried catalysts. It is shown as an example of how the sphericity can be controlled through the use of the appropriate spray drying parameters. Operating outside the range of proper parameters leads to the loss of catalyst sphericity and formation of dimpled particles (Figure 1b).
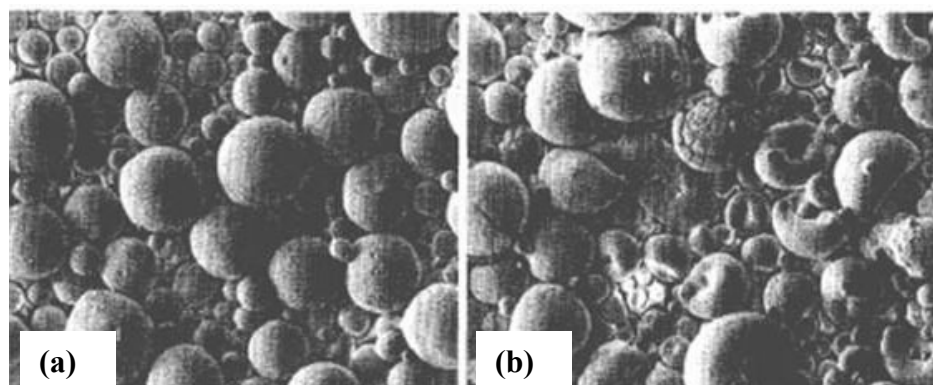
Figure 1. SEM images of spray dried iron catalysts prepared at Sasol. (a) Typical Sasol spray dried catalyst (b) Catalyst with dimpled particles. (From Jager and Espinoza [5]).

Findings on iron catalysts attrition resistance

Recently, several research groups have conducted studies on attrition phenomena. Professor Datye's group at the University of New Mexico (UNM) found that attrition occurs at two different scales, micro- and nano-scale. The nano-scale attrition is caused

by the volume changes that occur during the phase transformation of the oxide precursor into reduced iron species (α-Fe or iron carbides), which have lower specific volumes [10, 11]. They have also performed studies on measurement of attrition properties by subjecting particles to ultrasound energy and measuring particle size distribution after different periods of exposure to ultrasonic fragmentation [11, 12]. Their results showed that a precipitated iron catalyst had poor mechanical integrity, while some supports (alumina) did not show significant breakage of the primary particles [12]. They also studied attrition properties of spray dried iron catalysts. They reported that the use of spray drying technique results in improvement of the attrition resistance of Fe/Cu catalyst. Addition of silica binder to the Fe/Cu catalyst followed by spray drying resulted in further improvements of the attrition strength [13, 14].

Researchers at Hampton University (HU) and University of Pittsburgh (UP) have developed iron F-T catalysts with improved attrition resistance through addition of a silica binder followed by spray drying of the catalyst precursors. In their studies they used two series of catalysts: 1) Catalysts with nominal composition 100 Fe/ 5 Cu/4.2 K plus 4 to 20 wt. % of silica binder and 2) 100 Fe/5 Cu/4.2 K/ y SiO$_2$ (y= 5-20 parts per weight of precipitated silica) plus 12 wt. % silica binder [15-17]. The attrition properties of these catalysts (calcined after spray drying) were investigated using an air-jet attrition tester per ASTM-5757-95 standard [18]. Their findings showed that the attrition resistance increases with the addition of a silica binder up to 12 wt. %, but then begins to decrease with further addition of the binder. Catalysts containing 12 wt. % of silica binder plus precipitated silica exhibited a decrease in the attrition resistance as the amount of precipitated silica increased. Results obtained with these two series of catalysts showed that the attrition resistance is independent of the source of silica (binder or binder plus precipitated silica) for total silica contents greater than 12 wt. %. Their findings indicate that there is an optimum amount of silica binder for the maximum attrition strength. In a recent study [16] it was shown that spray dried precipitated iron

catalysts have higher attrition strength than the corresponding catalysts prepared using binder (colloidal) silica, for silica contents less than 12 wt. %.

The above studies of attrition properties of catalysts provide information on relative physical attrition resistance of different materials. However, these studies were not conducted under conditions encountered in a SBCR and/or in a stirred tank slurry reactor (STSR), and it is not clear whether these results can be used to predict the attrition behavior of catalysts in slurry reactors. In addition, they do not provide information on the catalyst attrition resistance after activation using hydrogen, carbon monoxide or syngas during F-T synthesis, i.e. during periods where the catalyst undergoes chemical changes (chemical attrition).

Performance of iron catalysts prepared at TAMU
Promoted iron catalysts are ideally suited for F-T synthesis with coal derived (CO rich) feed gas, due to their excellent water gas shift (WGS) activity. They are relatively inexpensive and have high selectivity to liquid hydrocarbons and wax. Highly active iron catalysts are prepared by precipitation [19-21]. However, there is concern that precipitated catalysts are structurally too weak and that they may break apart into fine particles during F-T synthesis in slurry reactors. These fine particles are difficult to separate from wax, and can cause plugging problems of downstream processes and contamination of final products. Also, precipitated catalyst particles are of irregular shape, and because of that are more likely to break into small particles by physical attrition.

Professor Bukur's group has been working on development of improved iron catalyst for F-T synthesis since 1984. Some of the promoted iron catalysts synthesized at TAMU (precipitated catalysts) have been found to be more active than iron catalysts used by Mobil [22] and Rheinpreussen [23] in two of their most successful SBCR tests. As it is shown in Table 1, TAMU's catalyst exhibits excellent catalytic performance with low methane selectivity (3 to 3.9 wt. %) at a total syngas conversion of about 78%. This

catalyst is more active and has significantly higher productivity than the catalysts developed by Mobil and Rheinpreussen, while its C_{5+} hydrocarbon selectivity is similar to that of Mobil's catalyst.   Detailed discussion and comparisons can be found in [21].

Table 1. Comparison of catalyst performance in slurry reactor tests. (Adapted from Bukur and Lang [21])

Reactor type [a]	Catalyst			
	STSR		SBCR	
	TAMU [b]		Mobil [22]	Rheinpreussen [23]
Test Conditions [c]				
Pressure, MPa	1.5	2.2	1.5	1.2
Space Velocity, Nl/g-Fe/h	3.9	5.8	2.3	3.1
Time on stream	145	314	475	
CO conversion, %	81	84	90	91
$(H_2 + CO)$ conversion, %	77	79	82	89
Hydrocarbon selectivities, wt.%				
CH_4	3.9	3.0	2.7	3.2 [d]
C_2-C_4	15.9	14.1	11.1	31.3
C_{5+}	80.3	82.9	86.2	65.5
C_1-C_2	8.3	7.0	5.6	6.8
Productivities				
Nm^3/kg-Fe/h	3.0	4.5	1.9	2.8
g HC/g-Fe/h	0.58	0.86	0.39	0.49

[a] STSR stands for Stirred Tank Slurry Reactor and SBCR stands for Slurry Bubble Column Reactor

[b] 100 Fe/3 Cu/4 K/16 SiO_2.   [c] TAMU tests: 260ºC, H_2/CO= 0.67-0.69, Mobil: 257ºC, H_2/CO= 0.73. Rheinpreussen: 268 ºC, H_2/CO= 0.67.

[d] CH_4 +C_2H_6.

Results obtained at Texas A&M University have demonstrated that catalysts, 100 Fe/3 Cu/4 K/16 SiO_2 and 100 Fe/5 Cu/4 K/24 SiO_2, have high activity and suitable product distribution for conversion of CO rich synthesis gas to hydrocarbon liquids. Now, the next step is to improve the attrition strength of these catalysts while maintaining their excellent catalytic properties.

BACKGROUND

Attrition

Particle attrition or in general terms, attrition can be defined as the fractionation of solid particles, or generation of fine particles from an initial unique solid piece [24]. This unwanted breakdown of solid particles is a frequently encountered problem in the development of suitable catalysts for use in catalytic chemical reactors. Examples of problems related with catalyst attrition may be summarized as follows: loss of catalyst as a consequence of fines generation, change of bulk properties of the catalyst and decrease in the final quality of the product due to separation problems.

In general, attrition resistance is affected by several factors related to the intrinsic properties of the particle and the environment that surrounds it (see Figure 2). Among the particle properties that affect the attrition strength are the size distribution, shape, porosity, surface, cracks and hardness of the particles. On the other hand, the conditions or environment surrounding the particles such as time of exposure, shear, velocity, pressure and temperature also are important in determining the severity of attrition [25]. Even though there have been several studies about particle attrition, it is clear that attrition is a quite complex phenomenon. Therefore, each system has to be specifically studied in order to adequately explain its attrition behavior and quantify it.
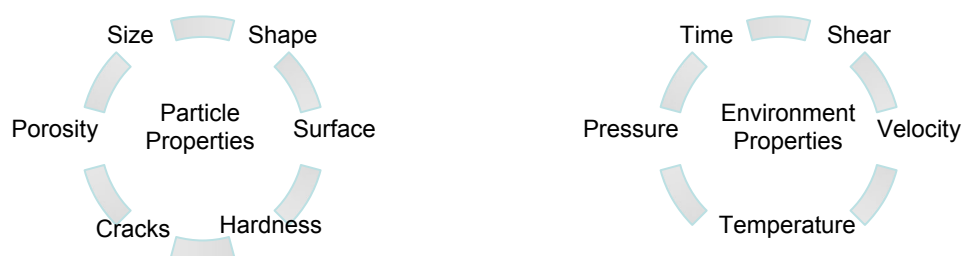
Figure 2. Examples of factors affecting attrition resistance. (Adapted from Bemrose and Bridgwater [25]).

Attrition of iron Fischer-Tropsch catalysts

Attrition of Fischer-Tropsch iron catalysts is believed to occur at two different scales, nano- and micro-scale, as proposed by professor Datye's research group at the University of New Mexico (UNM). The nano-scale breakage of iron catalysts is caused by the volume changes that occur during the phase transformation of the oxide precursor into reduced iron species, such as alpha-iron and iron carbides (chemical attrition) [10-11]. On the other hand, micro-scale attrition is caused by abrasion and erosion effects due to collisions between fast-moving particles or between the particles and the reactor walls (physical attrition) [25]. During physical attrition, the surface of the particles or their edges are removed, and complete destruction of the primary particles is possible due to fragmentation.

During F-T synthesis the environment, in which an iron catalyst is exposed, is defined by the reactor type used and the operating conditions (i.e. TFBRs, SBCRs or STSRs). On the other hand, the nature of catalyst attrition is highly influenced by the composition of the catalyst and the procedures employed to synthesize it. These factors will define the particles properties and therefore their attrition resistance. For instance, precipitated iron catalysts are commonly formed of irregular particles and there is concern that they may be structurally too weak compared to iron catalysts prepared by spray drying technique. As stated above, the formation of spherical particles by spray drying was

essential for maintaining their mechanical integrity during F-T synthesis [5]. Additionally, the likelihood of a specific particle breaking is also affected by the presence of cracks, which is related to the catalyst composition, i.e. whether a silica source is employed or not.

Attrition testing methods

Catalyst attrition in slurry reactors is a complex phenomenon, which has been studied in recent years. Simultaneously, and as a result of these studies, several types of attrition evaluation methods have been developed to measure the catalyst attrition resistance employing various instruments and procedures (e.g. compression test, rotating drum test, fluidized bed tests: air-jet test and jet-cup test).

Recently, research groups at University of New Mexico (UNM), Hampton University (HU) and University of Pittsburgh (UP) have been working on attrition assessment of F-T iron catalysts for use in SBCRs. They have explored different methods to evaluate attrition behavior of iron catalysts during F-T synthesis. Researchers at UNM have performed studies using ultrasonic test [10, 12, 14] and uniaxial compaction method [12]; whereas researchers at HU and UP have reported attrition studies using ultrasonic test, ASTM Standard Fluidized Bed test and Jet-Cup test [15-17, 26, 27]. These attrition resistance tests are briefly described below.

Uniaxial compaction method

Compaction is a method in which individual sample particles are crushed between 2 plates that provides increasing compression stress. The point of rupture under static stress determines the maximum stress that the material can sustain, defined as the compressive strength of the particle. Researchers at UNM performed studies using slight modification of the compression test, the so-called uniaxial compaction method in which a sample confined in a cylindrical die is compressed under load using an Instron 5565 machine. Treatment of both compactation and uniaxial compactation results can provide

average values of particle strength under static stresses. However, relation of this static strength to attrition strength of particles used in a SBCR or a STSR has not been established [12, 25].

Ultrasonic test

Particle breakage under controlled ultrasonic forces has been used by researchers at UP and UNM to evaluate attrition strength of F-T catalysts [10, 12, 14, 15, 28]. This test is founded on the fact that ultrasonic forces can induce intense cavitation stresses on solid particles suspended in liquid medium. Ultrasonic forces are dependent upon frequency and amplitude of the ultrasonic waves, physical properties of the suspension medium and medium temperature. Dr. Goodwin and co-workers at UP worked on the development of attrition resistant catalysts for F-T synthesis and reproducibility of attrition conditions present in SBCRs using a 20 kHz Tekmar TM501 Sonic Disrupter. In their work, it was found that under optimal operating conditions, ultrasonic test produced attrition results quite similar to those obtained in the slurry bubble column reactor. However, this test is considered to be slightly inferior relative to the jet cup test used in studies at UP [15, 28].

Dr. Datye's research group (UNM), performed attrition studies of F-T iron catalysts with a calibrated ultrasonic field using a 20 kHz Tekmar TSD-500 Sonic Disrupter to determine the catalyst strength, and a Micromeritics Sedigraph 5100 analyzer to measure the particle size distributions before and after sonication. Their findings were that particle breakdown is associated with two attrition mechanisms, erosion and fracture. Erosion is a process where primary particles are dislodged from the surface of the agglomerate. Fracture is the division of the original agglomerate into several smaller agglomerates, and results from crack propagation through the agglomerate [10, 12, 14].

Jet-cup test

In this attrition test, sample particles are carried by a high velocity air stream. Here particles agitate first in a small cup and then in a cyclone type chamber. The induced movement of particles by high velocity air flow leads to particle-particle and particle-walls collisions, which eventually results in particle attrition. Weeks and Dumbill [29] compared jet-cup test against fluidized test and concluded that the jet-cup test was more effective to measure attrition and that the *attrition rate* was independent of testing time. This time independence was also observed in attrition studies performed at HU and PU, and it suggests that the attrition associated with jet-cup test is primarily due to fracture mechanism [30].

ASTM standard fluidized test

Fluidized bed tests are widely used to assess material attrition behavior, especially where materials are intended for use under fluidized conditions. Forsyte and Hertwing [31] were the first to develop a high-velocity air-jet attrition apparatus and their work became basis for subsequent modifications [18, 32-34]. Attrition behavior for fluidized beds test is dependent upon parameters such as time, particle size, gas velocity, bed length and temperature. Attrition rate then can be expressed as a function of all the parameters listed above and in general terms it is expressed as:

$$r_{attrition} \propto (H^m \, \rho_f \, \rho_s \, U_o^n \, \Delta T_f) \, (t^e \, D_p^g)^{-1}$$

Induced particle breakage mechanisms in air-jet test are believed to be fracture (in the grid region of the apparatus) and abrasion (in the bubble zone of the apparatus) [25]. Studies performed at PU with spray-dried iron catalysts confirmed the time dependency of the attrition, suggesting that air-jet tests are related to abrasion mechanisms [30, 32].

Dr. Goodwin's research group (PU) has performed attrition studies of spray-dried iron catalyst using both jet-cup and ASTM standard fluidized bed tests. In their work the

extent of attrition was defined as the weight percent of fines (particles < 20 μm) generated after attrition test (weight percent of fines = [weight of fines generated/weight of total catalyst] *100). Their conclusions point to the fact that the jet-cup test produced very similar results to the ones obtained from the ASTM standard fluidized bed test. Therefore, the jet-cup test can be used for catalyst attrition prediction, even though the attrition mechanisms in these two types of tests are not identical [30].

All the attrition tests listed above have been used to evaluate the attrition strength of iron catalyst for the F-T synthesis. However, none of them reproduce entirely the conditions present in slurry reactors.

Spray drying technology

By definition, *spray drying* is the transformation of feed from a fluid state, which can be a slurry, suspension or solution into a dried form by spraying the feed into a hot drying medium. Spray drying involves the formation of dry solids in either powder, granulate or agglomerate form, depending upon the physical and chemical properties of the feed, the drying parameters and the dryer design [35].

A typical spray dryer consists of the following main components:
  - Drying chamber,
  - Hot air system and air distribution,
  - Feed system,
  - Atomizing device and
  - Powder separation system

Specific design of each of these components defines the operational flexibility of spray dryers, and because of that, they will restrict the drying parameters that can be modified to obtain dried products with the desired properties. The end product generally has to

comply with quality standards such as particle density, friability, dispersibility and moisture content.

Operational parameters affecting spray-dried product morphology

The effect of operational parameters upon particle morphology, i.e. the residence time of particles within the drying chamber, type of spray/hot air contact, the method and conditions of atomization, the drying air temperature and the feed parameters such as concentration and temperature, has to be analyzed for each particular system, since there are no general correlations that cover all possible materials and applications for spray drying technique.

Residence time depends on the chamber dimensions and hot air flow, whereas the type of spray/hot air contact is defined by the way the spray dryer is operated. Dryers are usually operated either in co-current flow, mixed flow or counter-current flow. In the latter mode, the drying air and particles move through the drying chamber in opposite directions. In co-current flow, both the drying air and particles move through the chamber in the same direction. In contrast, mixed flow implies the movement of particles through the chamber in both co-current and counter-current modes. In all three cases, the movement of air predetermines the rate and degree of evaporation by influencing the passage spray through the drying zone, the concentration of product in the region of the dryer walls and the extent to which semi-dried droplets re-enter the hot areas around the dispenser. Additionally, selection of the right atomization system (i.e. pressure nozzle atomizer, rotary atomizer or two fluid nozzles) depends upon the nature of the feed and desired characteristics of the dried product (i.e. morphology and particle size distribution) [36].

Parameters already described above, have crucial effect upon the morphology and particle size distribution of the dried products. However, they can not be altered during a normal operation since they are controlled by the spray dryer mechanical design. On the

other hand, parameters such as feed concentration and drying temperature (see Table 2) can be modified from one experimental run to another, giving some flexibility to modify the properties of the final product. Therefore, experimental optimization studies can be performed according to the type of material being spray dried, and the particle or powder specifications required.

Table 2. Effect of the feed concentration and drying temperature upon the morphology of the dried powders. (Adapted from Walton [36])

Increased feed concentration:	Increased drying temperature:
Decreases surface irregularities	Decreases drying time
Increases the particle size	Increases the particle size
Reduces thermal degradation	Decreases bulk density
Increases bulk density	Increases particle vacuolation
Decreases particle vacuolation	

Particle size measurements

Particle size and distribution are important in a large number of practical applications, because of their effect on mechanical properties such as packing and flowing. In many cases the materials are useful only at specific size distributions. Therefore several characterizations techniques have been developed in order to quantify the particle size distributions. Among techniques employed for particle size analyses are: sieving, microscopy, sedimentation, centrifugal, optical and electrical sensing zone methods. Each of these techniques provides valuable information about the PSD. Unfortunately, there is no single technique that can adequately cover all possible applications. The sizing technique has to be selected according to the specific requirements of a given situation.

Methods of representing PSD results

The methods of expressing particle size depend on the technique used, as well as, the purpose of the measurement. Spherical particles are completely defined by their diameter. However, not all particles are spherical and for irregular particles the assigned size depends on the method of measurement. Hence, it is necessary to define an "equivalent diameter" to describe size of non-spherical particles. On the other hand, because not all particle sizing methods respond in the same way to the shape and orientation of particles, it should not be surprising that the equivalent diameter varies according to the technique used. Table 3 provides some definitions of particle size, which are commonly applied to an assembly of particles and distributions in terms of the measured or derived diameters [37].

Table 3. Some definitions of particle size. (Adapted from Allen [37])

Name	Symbol	Formula	Definition
Volume diameter	d_v	$V = \pi/6 \, d_v^3$	Diameter of a sphere having the same volume as the particle.
Surface diameter	d_s	$S = \pi \, d_s^2$	Diameter of a sphere having the same surface as the particle.
Surface-Volume diameter	d_{sv}	$d_{sv} = d_v^3/d_s^2$	Diameter of a sphere having the same external surface to volume ratio as a sphere.
Projected area diameter	d_a	$A = 4d_a^2/\pi$	Diameter of a circle having the same area as the projected area of the particle resting in a stable position.

Results obtained from particle sizing are reported as average values, due to the simplicity of this way to represent in a concise manner the characteristic features of the group of particles. There are many definitions for average diameter, but all of them are a measure of central tendency which is unaffected by the extreme values in the tails of the distribution [37]. Table 4 provides some definitions of average diameters, selection of

one definition or other depends upon the specific requirements for a particular application.

Table 4. Examples of average diameters commonly used. (From Allen [37])

Name	Symbol	Definition [$]
Number, length diameter	d_{NL}	$d_{NL} = \dfrac{\sum \mathrm{d}L}{\sum \mathrm{d}N} = \dfrac{\sum d\,\mathrm{d}N}{\sum \mathrm{d}N}$
Surface, volume mean diameter (Sauter mean diameter)	d_{SV} ($d_{3,2}$)	$d_{SV} = \dfrac{\sum \mathrm{d}V}{\sum \mathrm{d}S} = \dfrac{\sum d^3 \mathrm{d}N}{\sum d^2 \mathrm{d}N}$
Volume, moment mean diameter	d_{VM}	$d_{VM} = \dfrac{\sum \mathrm{d}M}{\sum \mathrm{d}V} = \dfrac{\sum d^4 \mathrm{d}N}{\sum d^3 \mathrm{d}N}$
Weight, moment mean diameter	d_{WM} ($d_{4,3}$)	$d_{WM} = d_{4,3} = \dfrac{\sum \mathrm{d}M}{\sum \mathrm{d}W} = \dfrac{\sum d\,\mathrm{d}W}{\sum \mathrm{d}W} = \dfrac{\sum d^4 \mathrm{d}N}{\sum d^3 \mathrm{d}N}$

[$] dL, dV, dM, dW and dN are the differential change in particle length dimension, volume, mass, weight and number, respectively.

The Coulter Counter Multisizer analyzer

Measurement of particle size distribution (PSD) of F-T catalysts prepared in this study was the main tool to obtain quantitative information about their attrition resistance after reaction tests in a STSR. Most of PSD measurements for the catalysts prepared and/or tested in this work were performed using a Coulter Counter Multisizer analyzer. This instrument uses the so-called "Coulter principle" or electrical sensing zone method to size particles. Fundamentals of this instrument are briefly described below.

The Coulter principle – fundamentals

The Coulter Counter Multisizer determines the number and size of particles suspended in a conductive solution (i. e. Isoton II from Beckman-Coulter) by causing them to pass through a small aperture on either side of which is submerged an electrode (see detail in Figure 3). The changes in electrical impedance as particles are swept through the aperture of known diameter and length generate voltage pulses whose amplitudes are proportional to the particles' volume. Then, the pulses are amplified, sized and counted and finally the diameter of the particle can be computed from the obtained data [37].
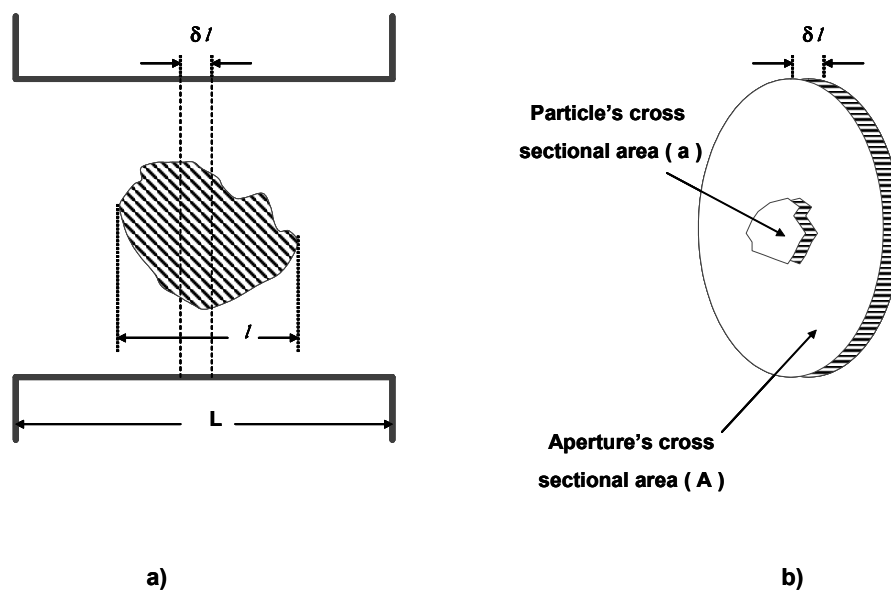
Figure 3. Aperture of the Coulter[®] Counter Multisizer. a) Detail of one particle passing through the aperture and b) differential section of the particle and the aperture. (From Allen [37]).

As described above, the Coulter Counter Multisizer operates under the assumption that the voltage pulse generated when a particle passes through the aperture, is related

directly the volume of the particle [37]. This relationship can be explained using Figure 3, which shows a detail of one particle passing through the aperture (a), and an element of one particle and the aperture (b). Then, the resistance of element without a particle, δR_o, is given by:

$$\delta R_o = (\rho_f \delta l) A \quad \cdots\cdots\cdots\cdots\cdots\cdots\cdots\cdots\cdots\cdots\cdots \quad (1)$$

In the same way, the resistance of the element including a particle is:

$$\delta R = \cfrac{1}{\cfrac{A-a}{\rho_f \delta l} + \cfrac{a}{\rho_s \delta l}} \quad \cdots\cdots\cdots\cdots\cdots\cdots\cdots\cdots\cdots \quad (2)$$

Where ρ_f and ρ_s are the resistivities of the particle and conductive solution respectively. Subsequently, the change in the resistance of the element because of the presence of the particle, $\delta(\Delta R)$, can be estimated as follows:

$$\delta(\Delta R) = (\delta R_o - \delta R) \quad \cdots\cdots\cdots\cdots\cdots\cdots\cdots\cdots \quad (3)$$

Substituting equations 1 and 2 into equation 3,

$$\delta(\Delta R) = (\rho_f \delta l) A - \cfrac{1}{\cfrac{A-a}{\rho_f \delta l} + \cfrac{a}{\rho_s \delta l}} \quad \cdots\cdots\cdots\cdots\cdots\cdots \quad (4)$$

Then, combining terms, equation 4 becomes:

$$\delta(\Delta R) = \cfrac{(-\rho_f a \delta l)}{A^2} \cdot \cfrac{\left(1 - \cfrac{\rho_f}{\rho_s}\right)}{\left(1 - \left[1 - \cfrac{\rho_f}{\rho_s}\right]\cfrac{a}{A}\right)} \quad \cdots\cdots\cdots\cdots\cdots \quad (5)$$

The term ρ_f / ρ_s in equation 5 can be neglected since, in practice, the response is independent of the particle's resistivity and it is suggested that the electrical resistivity of the particles is very large ($\rho_s \approx \infty$) [37, 38]. Therefore, the equation 5 can be simplified as follows:

$$\delta(\Delta R) = -\frac{\rho_f a \delta l}{A^2} \cdot \frac{1}{\left(1 - \dfrac{a}{A}\right)} \qquad \text{............................} \text{ (6)}$$

For spherical particles (radius = r), the change in resistance due to an element of thickness δl at the distance l from the center of the sphere (see Figure 4) can be estimated from the following equation:

$$\Delta R = -\frac{2\rho_f a \pi^2}{A} \cdot \frac{\left(r^2 - l^2\right)}{\left(1 - \dfrac{\pi\left(r^2 - l^2\right)}{A}\right)} \delta l \qquad \text{..........................} \text{ (7)}$$
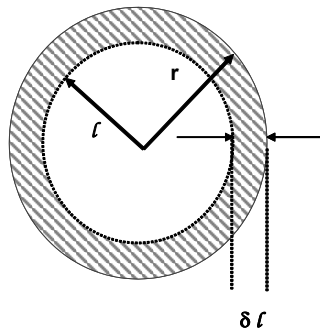
Figure 4. Front view of a sphere with radius, r, and an element of thickness, δl, at the distance, l, from the center of the sphere.

T. Allen [37] reports a solution for this equation in terms of the diameter of the sphere, *d*, (see equations 8 and 9). Equation 9 shows that the response is proportional to the volume of the sphere times the function F_1. Additionally T. Allen provides a brief description of solutions that have been proposed for this function.

$$\Delta R = -\frac{4\rho_f}{\pi D} \cdot \left(\frac{\sin^{-1}(d/D)}{\sqrt{1-(d/D)^2}} - \frac{d}{D} \right) \quad \text{.............................. (8)}$$

or

$$\Delta R = \rho_f \frac{v}{A^2} F_1 \quad \text{................................. (9)}$$

The PSD results obtained using the Coulter® principle for spherical particles are in good agreement with other techniques. However, for non-spherical particles the results obtained from different techniques may differ [39, 40].

EXPERIMENTAL

Catalyst synthesis: Hampton University and Ruhrchemie catalysts

Three catalysts prepared at HU were used in this study, two of them containing precipitated silica (100 Fe/5 Cu/4.2 K/11 SiO_2 and 100 Fe/3 Cu/4 K/16 SiO_2), and the other containing silica binder (100 Fe/5Cu/4.2 K/1.1 SiO_2). The preparation procedure for each of these catalysts was not provided to our research group. However, procedures for catalysts synthesis with similar compositions to the ones used here were reported in the literature [17].

According to the procedure described in [17], the catalysts containing binder silica were prepared by the simultaneous coprecipitation of iron nitrate and copper nitrate. This coprecipitation was carried out at constant pH using an aqueous ammonia solution to prepare the Fe/Cu precursor. The precipitate was then washed with deionized water by vacuum filtration. Afterward, the potassium promoter was added as aqueous potassium bicarbonate solution to the undried, reslurried Fe/Cu precursor. Subsequently, silica binder was added to this precursor, but the binder preparation and addition method were not detailed because of its proprietary nature. Finally the catalysts were spray dried at 250ºC using a bench-scale Niro spray dryer (0.90 m in diameter and 1.8 m height) and calcined in a muffle furnace at 300 ºC for 5 hours.

Catalysts containing precipitated silica were prepared in a similar way to that described above, but the silica was introduced as an aqueous tetraethyl orthosilicate solution (TEOS). This procedure involves precipitation of Fe/Cu/SiO_2 precursor from a flowing aqueous solution containing iron nitrate, copper nitrate and TEOS using aqueous ammonia; incorporation of potassium; spray drying and calcination as described above.

A commercial catalyst (Ruhrchemie catalyst) with composition 100 Fe/5 Cu/4.2 K/25 SiO_2 was also used in this study. Catalyst preparation procedure was amply described by Frohning et al. [41] and summarized by Dry [2]. Briefly, the catalyst synthesis steps can be listed as follows: (1) Coprecipitation of Fe/Cu precursor from a near boiling aqueous solution of iron and copper nitrate using a hot solution of sodium carbonate; (2) washing/filtration of the Fe/Cu precursor to eliminate the sodium ions; (3) addition of the desired amount of silica from a potassium waterglass solution (sodium silicate) to prepare the $Fe/Cu/SiO_2$ precursor; (4) Addition of nitric acid to remove some of the excess potassium so that after filtration the desired $Fe/Cu/K/SiO_2$ ratio was obtained [2]. Table 5 shows specific details for HU catalysts and the Ruhrchemie catalyst.

Table 5. Catalysts prepared at Hampton University and Ruhrchemie catalyst

Catalyst composition*	Silica Source	Designation
100 Fe/5 Cu/4.2 K/11 SiO_2	Precipitated (from TEOS)	HU2061
100 Fe/3 Cu/4 K/16 SiO_2	Precipitated (from TEOS)	HU1112
100 Fe/5Cu/4.2 K/1.1 SiO_2	Silica Binder	HU3471
100 Fe/5Cu/4.2 K/25 SiO_2	Precipitated (from Sodium Silicate)	CC3291

* Catalyst composition is given on mass basis.

Catalyst synthesis: TAMU catalysts

Precipitated iron catalysts

The procedure used to prepare iron catalysts containing precipitated silica can be found in [42, 43], and it consists of several steps: (1) coprecipitation of Fe/Cu precursor; (2) incorporation of silica binder; and (3) impregnation by potassium promoter (Figure 5). Specific details of the catalyst synthesis procedures are given below.

23
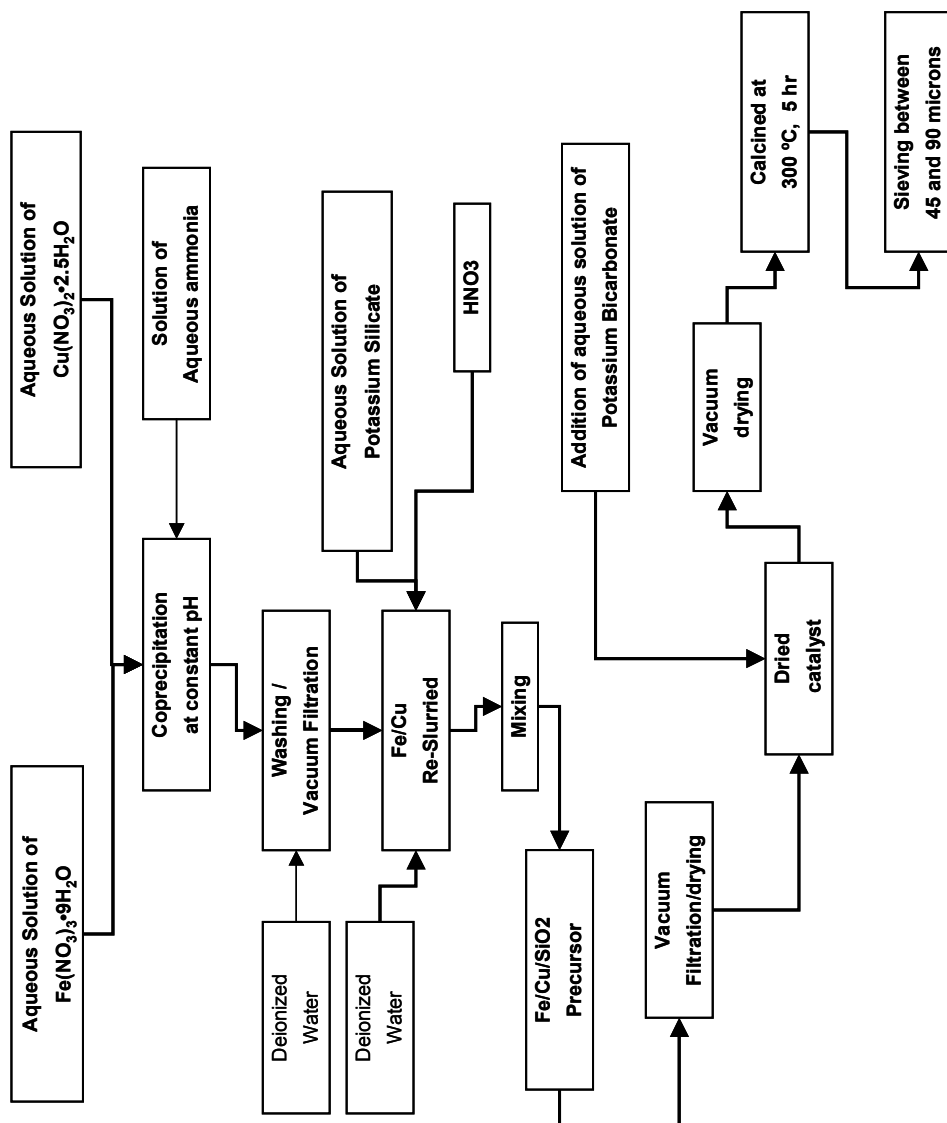
Figure 5. Schematics of the precipitated catalyst synthesis procedure using potassium silicate as the silica source.

Coprecipitation of Fe/Cu precursor

An aqueous solution (~0.6 M) containing ferric nitrate nona-hydrated (J. T. Baker) and copper nitrate 2.5-hydrated (J. T. Baker) at the desired ratio Fe/Cu in the final catalyst, and a second aqueous solution (~2.7 M) containing aqueous ammonia (Mallinckrodt) were maintained in stirred round-bottom flasks at 85 ± 2 ºC and 78 ± 2 ºC respectively. These solutions were separately pumped to a stirred tubular glass reactor (Figure 6) maintained at constant temperature (82 ± 2 ºC). The coprecipitation was carried out continuously as the two solutions were pumped upward through the reactor, while the pH was monitored with an in-line pH electrode at the reactor outlet. The coprecipitate was collected only at a pH value of 6.0 ± 0.3. Then, the coprecipitate was chilled in Nalgene beakers and thoroughly washed with distilled/deionized water by vacuum filtration to remove the excess ammonia and nitrate ions.
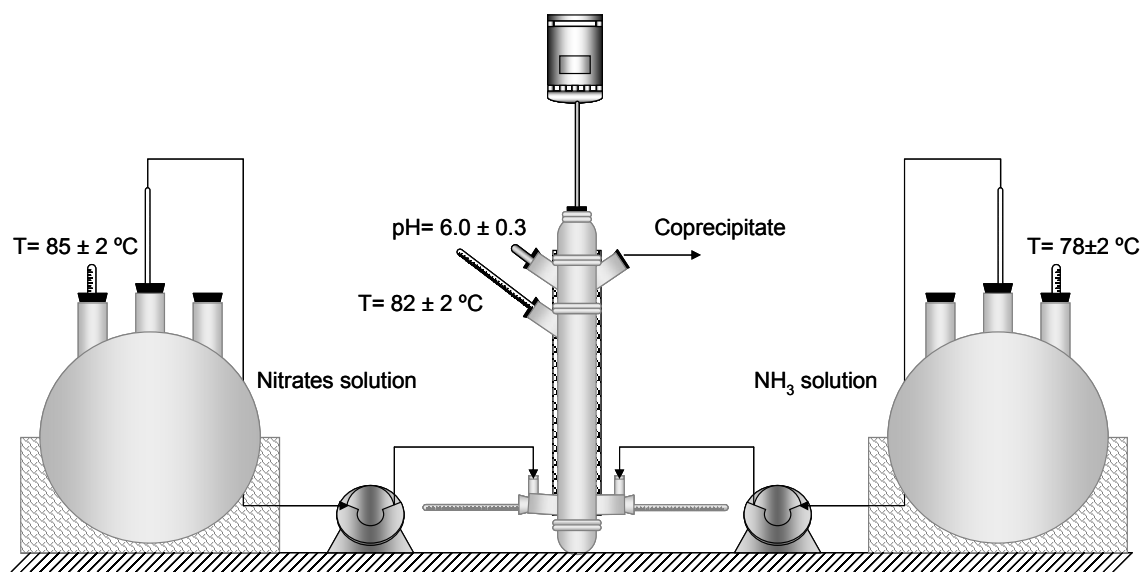
Figure 6. Continuous precipitation equipment used for synthesis of iron catalysts.

Addition of SiO₂ from potassium silicate

The Fe/Cu coprecipitate obtained was then reslurried and SiO_2 was introduced from an aqueous potassium silicate solution, which was subsequently decomposed by addition of nitric acid to produce SiO_2. During potassium silicate addition the pH was maintained at about 9.0. Once the addition of potassium silicate was over and the pH stabilized, a 10% dilute nitric acid was added drop by drop until the pH reached ~ 6.0 with constant stirring. Stirring was continued for additional four hours after the addition of nitric acid. Immediately after completion of stirring procedure the resulting slurry was thoroughly washed with distilled/deionized water by vacuum filtration to remove the excess of potassium and nitrate ions. Finally, the $Fe/Cu/SiO_2$ precursor was vacuum dried at 50ºC for 4.5 hours and then at 120ºC for 24 hours.

Addition of potassium and catalyst drying

The $Fe/Cu/SiO_2$ precursor was impregnated with potassium promoter by addition (drop-wise) of the desired amount of aqueous potassium bicarbonate solution from an aqueous solution. The final step was to vacuum dry the catalyst at 120ºC for 16 hours.

Spray dried catalysts

Preparation of spray dried iron catalysts was done in several ways using: (1) vacuum-dried precipitated iron catalysts; or (2) wet precursors containing either precipitated silica (from K_2SiO_3 or TEOS); or (3) colloidal silica; or (4) precipitated silica (from K_2SiO_3) plus silica binder.

Preparation of spray dried catalysts from vacuum-dried precipitated iron catalysts

The first approach employed to prepare spray-dried iron catalysts was to start with a precipitated iron catalyst in its final form (vacuum-dried $Fe/Cu/K/SiO_2$ catalyst). This material was first sieved and the fraction which passed through a 325-mesh sieve (particles less than 45 μm in diameter) was collected and placed in a cylindrical can

(0.15 m in diameter and 0.20 m in height) filled with 30 metal balls (~6 mm in diameter). The can was placed in a tumbler for 5 h to reduce the catalyst particle size, due to friction and collision with walls and spherical balls (Figure 7). The resulting powder was mixed with water to form a slurry, which was sonicated at 40 kHz for 60 minutes in an ultrasonic bath (model FS14 from Fisher Scientific) to break up any agglomerates, and then spray dried as described below.
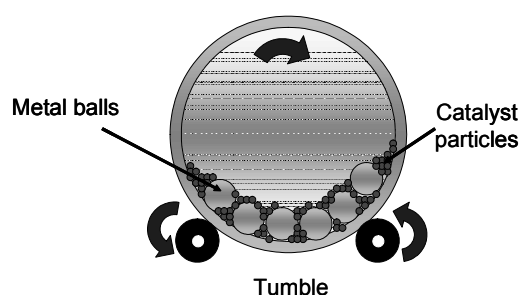
Figure 7. Schematic representation of the tumbler-can-metal balls device used to reduce the catalyst particle size.

The second approach was to prepare a catalyst containing both precipitated silica (from potassium silicate) and silica binder. A commercial silica binder from Akzo Nobel (Bindzil 30/360) was added to a slurry of precipitated catalyst (prepared as described above). The slurry was then sonicated for 60 minutes in an ultrasonic bath to break up any agglomerates. The resulting slurry was then spray dried. The additional amount of silica added (in the form of binder) was 3 wt. % of total catalyst weight. For example, the catalyst 100 Fe/3 Cu/6 K/16 SiO_2 plus 3 wt. % of silica binder has a total silica content in the final catalyst of about 12 wt. % (~9.1 wt. % precipitated SiO_2 from potassium silicate and ~2.9 wt. % of binder SiO_2).

Preparation of spray dried catalysts from wet precursors

The other procedures were based on the use of wet catalyst precursors (Fe/Cu or Fe/Cu/SiO$_2$) prepared as described previously for precipitated iron catalysts. For example, if one uses potassium silicate as the source of precipitated silica, it is possible to start with the wet Fe/Cu/SiO$_2$ precursor (after washing to remove excess K$^+$ and NO$_3^-$ ions). This precursor was reslurried using deionized water and the desired amount of potassium promoter was added drop-wise using an aqueous solution of potassium bicarbonate. Following the sonication step, the slurry was spray dried. On the other hand, it is also possible to add the potassium promoter after spray drying step, utilizing incipient wetness impregnation (I.W.I) method, followed by vacuum drying (Figure 8). Catalysts containing both precipitated and binder silica can be prepared using this procedure. Binder silica may be added before or after potassium addition to washed Fe/Cu/SiO$_2$ precursor.

Alternatively, tetraethyl orthosilicate (TEOS) or colloidal silica suspension can be used as the silica source instead of potassium silicate. In the latter case one starts with a Fe/Cu precursor prepared according to the procedure described for preparation of precipitated iron catalysts. The washed coprecipitate was reslurried using distilled/deionized water and desired amount of silica was added using a commercial colloidal silica suspension. Potassium promoter may be added to the Fe/Cu/SiO$_2$ precursor using an aqueous potassium bicarbonate solution (drop-wise and in wet form), followed by slurry sonication for one hour in an ultrasonic bath before the spray-drying step. Alternatively, Fe/Cu/SiO$_2$ precursor can be sonicated for one hour, spray dried, and then impregnated with potassium by I.W.I. method. Subsequently, the catalyst was dried in a vacuum oven (overnight) at 110 ºC (Figure 9).
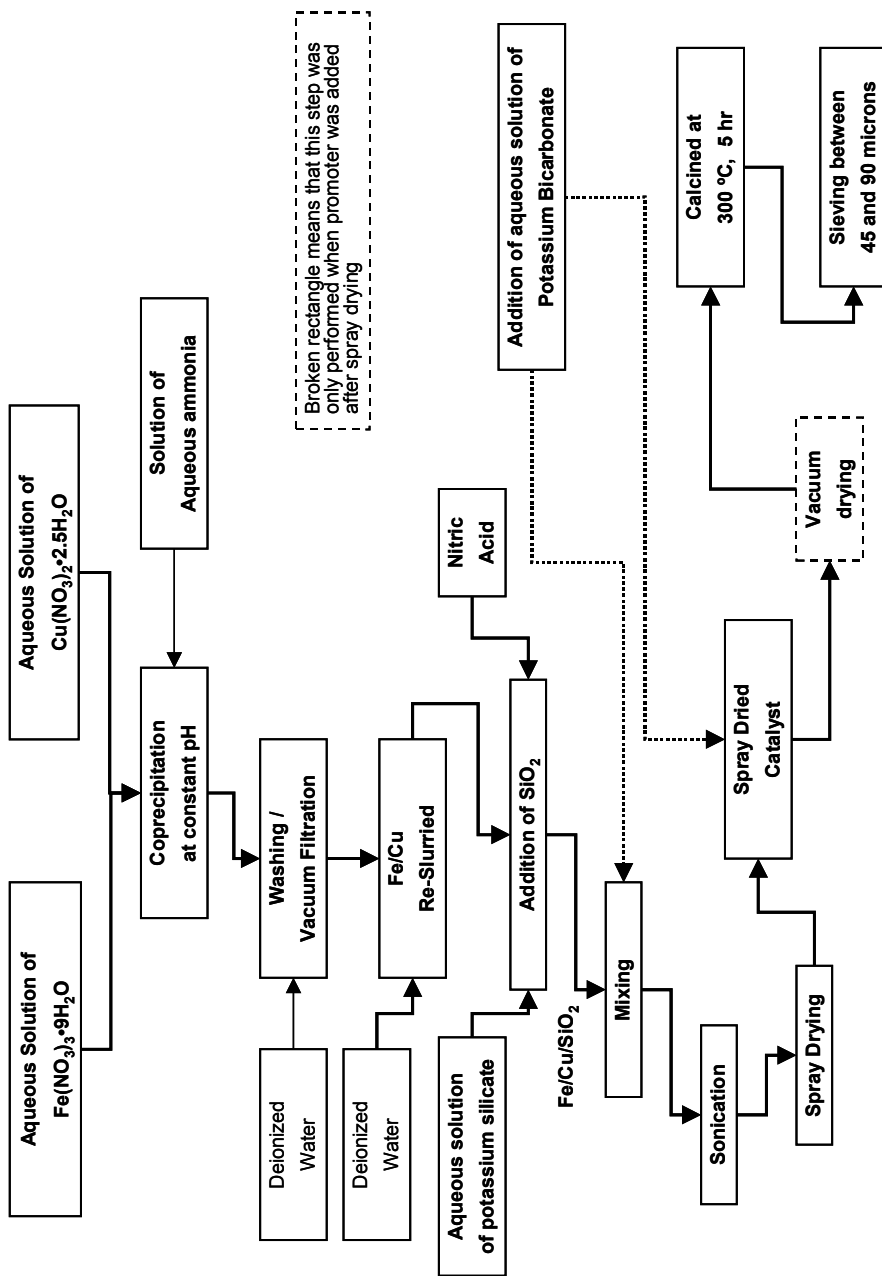
Figure 8. Schematics of the catalyst synthesis procedure using potassium silicate as the silica source.
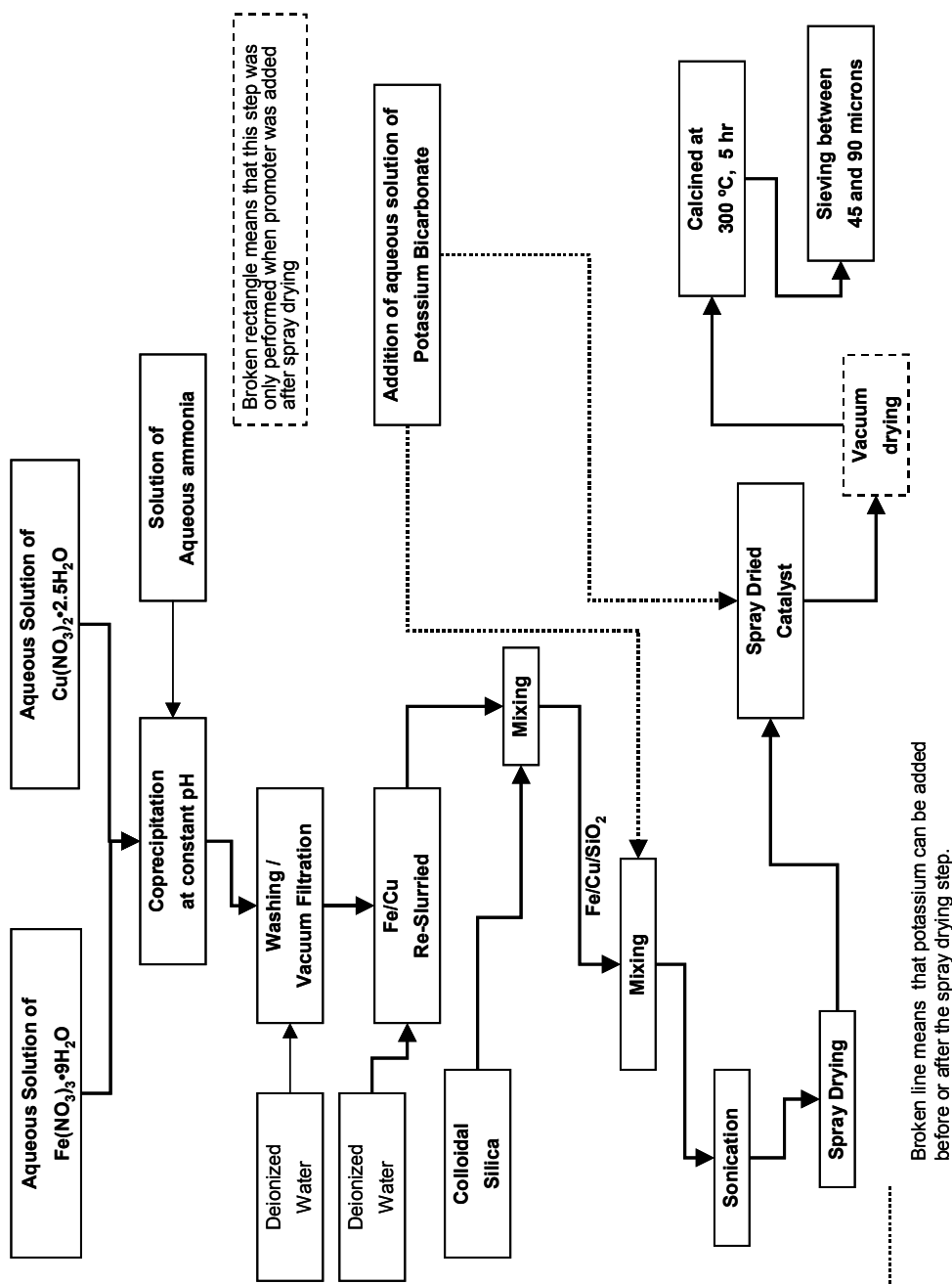
Figure 9. Schematics of the catalyst synthesis procedure using colloidal silica.

Finally, when TEOS was used as the source of silica, a slight modification of the synthesis procedure already described was employed. The $Fe/Cu/SiO_2$ precursor was obtained from simultaneous precipitation of ferric nitrate nona-hydrated, copper nitrate 2.5-hydrated and TEOS at the desired $Fe/Cu/SiO_2$ ratio in the final catalyst. Then the potassium promoter was added either in wet form before the spray-drying step, or by I.W.I. after spray drying (Figure 10).

Catalyst calcination

Catalyst samples were calcined under flowing air conditions in a glass tube reactor (~0.3 m in diameter) at 300 ºC for 5 hours. Alternatively, catalyst samples were calcined in stationary air using an Isotemp® Muffle Furnace 750 Series (Fisher Scientific) at 300 ºC for 5 hours.

Spray drying

Spray drying experiments were conducted at the Food and Protein Research Center at TAMU. Most of the tests were performed in an APV Anhydro Lab. S1 spray dryer (1.1 m in diameter and 2.4 m in height) with 6.8 kg/h of water removal capacity. A limited number of experiments were conducted in a bench scale APV Anhydro spray dryer (2.1 m in diameter and 2.4 m in height) with 29.5 kg/h of water removal capacity. Atomization system for both spray dryers consists of centrifugal wheel atomizers and peristaltic tubing pumps (Cole Parmer Instruments–Masterflex®). Both spray dryer units are operated in counter-current mode. The feed was pumped from the product feed tank to the atomizing device, which is located in the air dispenser at the top of the drying chamber. The drying air was drawn from the atmosphere via a filter by a supply fan and it passed through the air heater. Hot air was continuously fed to the drying chamber through the air dispenser placed at the top of the spray dryer unit. Catalyst recovery system consisted of a cyclone separator installed as shown in Figure 11.
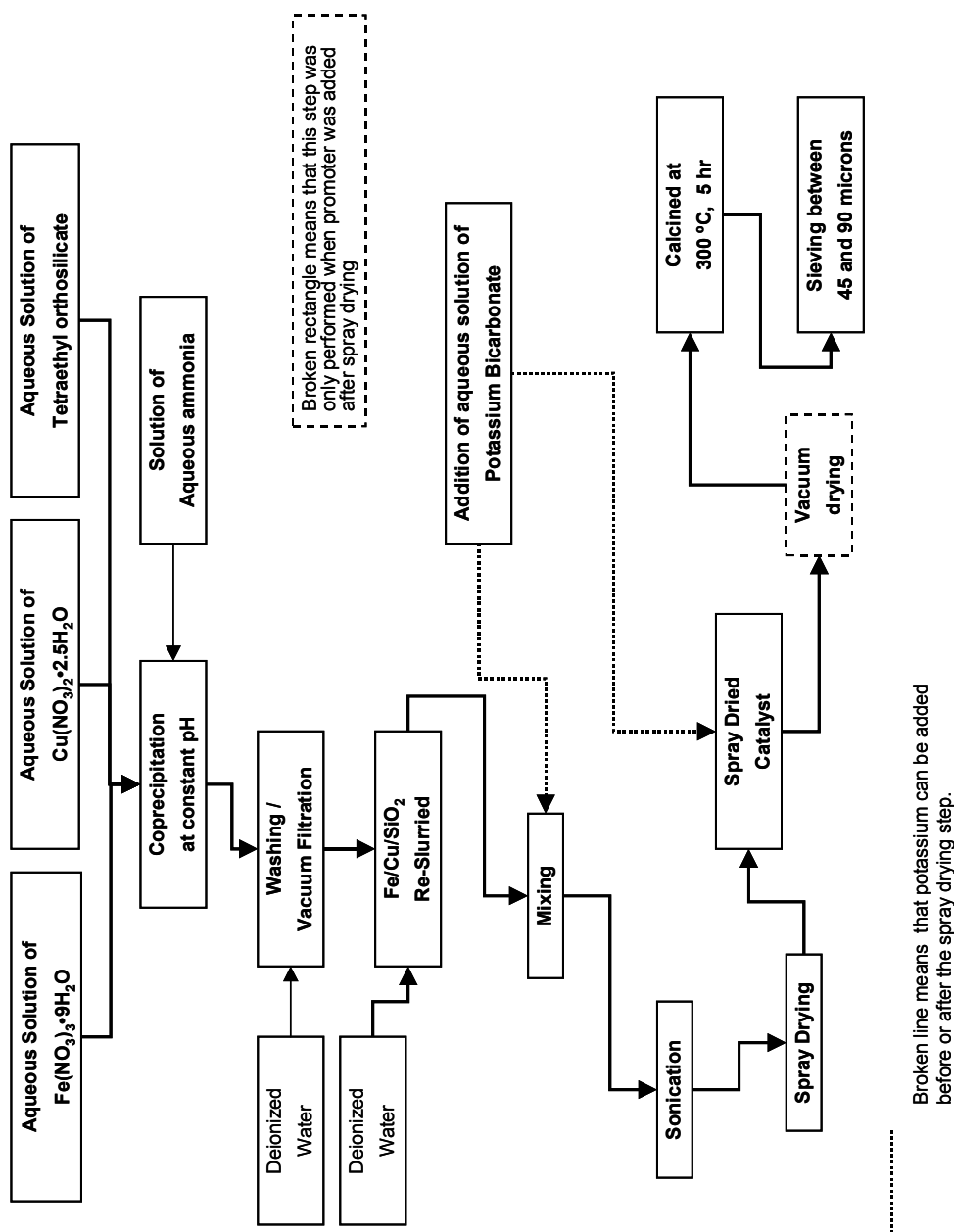
Figure 10. Schematics of the catalyst synthesis procedure using tetraethyl orthosilicate as the silica source.
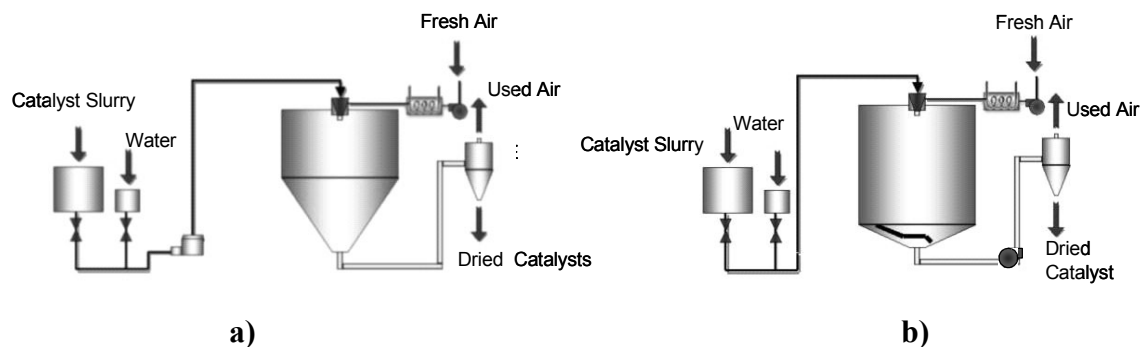
Figure 11. Schematics of (a) APV Anhydro Lab. S1 and (b) bench scale APV Anhydro spray dryers.

Spray drying operation

Typically, the spray drying operation begins by heating the apparatus with an air stream, adjusting the power input to achieve the desired inlet temperature (200/300 ºC), and feeding distilled water at the desired flow rate through the atomizer. After the desired operational parameters are adjusted and steady conditions are reached, the spray dryer is allowed to run for approximately 15 minutes. Subsequently, the feed stream is switched to catalyst slurry, which was kept suspended by mechanical agitation throughout the entire run. During the operation larger particles are collected at the bottom of a cyclone separator and the smaller ones are vented through the cyclone exit. The spray drying operation is concluded, when the catalyst slurry is consumed and dried catalyst particles collected at the bottom of the cyclone are removed.

Spray drying of model powders

Several spray-drying experiments were made using two model powder systems, iron oxide (Fe_2O_3) and iron oxide/binder silica (Bindzil 30/360). In the former case iron oxide powder was mixed with distilled/deionized water to form slurries containing 20-40 wt. % of total solids content, and then spray dried in the APV Anhydro Lab. S1 spray

dryer at 200-300ºC. In another set of experiments iron oxide was mixed with distilled/deionized water and commercial binder silica (Bindzil 30/360). The resulting slurry contained 11 wt. % of silica, based on the total weight of solid. Amount of silica added is similar to the silica content in TAMU's iron F-T catalysts (9-14 wt. % of SiO_2). The objectives of experiments with model powders were to gain experience with operation of the APV Anhydro Lab. S1 spray dryer and investigate the effect of slurry concentration and/or inlet temperature on morphology and particle size of spray-dried materials. Selection of iron oxide as a model powder material was based on the fact that iron F-T catalysts consist primarily of iron oxide (Fe_2O_3). However, it is understood that iron oxide in model powders and in F-T catalysts is not of the same nature (i.e. physical structure).

Catalyst description

Identification label for catalysts series prepared at TAMU consists of 3 capital letters, which indicate the preparation procedure, and a 5-digit number that shows the catalyst composition (see Table 6). The specific meanings for these letters and numbers are given below.

First capital letter:

P: Stands for precipitated catalysts (not spray dried).
D: Stands for spray dried catalysts from dry form.
W: Stands for spray dried catalysts from wet form.

Second and third capital letters:

PS: Stands for catalysts prepared using potassium silicate as the main source of SiO_2
CS: Stands for catalysts prepared using colloidal silica as the main source of SiO_2
TO: Stands for catalysts prepared using TEOS as the main source of SiO_2

The 5-digit number shows the catalyst composition by in parts per weight per 100 parts of iron. The first digit stands for Cu, the second one stands for K and the last two digits stand for SiO_2. When more than one catalyst of the same composition and method is prepared, the batch number is also given as the fifth digit after a hyphen. For instance, designation WCS3516-1 means that the catalyst 100 Fe/3 Cu/5 K/16 SiO_2 (batch 1) was spray dried from a wet precursor and the silica source was colloidal SiO_2.

Table 6. Catalyst series prepared at TAMU

Catalyst Series	Silica Source
WPS3516	Potassium Silicate
WCS3516	Colloidal Silica
WTO3516	Tetraethyl Orthosilicate
DPS3516	Potassium Silicate
DPS5624	Potassium Silicate
PPS3516	Potassium Silicate

Instrumentation and procedures

Catalyst sieving

Catalyst samples were normally sieved between 170 and 325 mesh (45-90 μm) using a mechanical shaker and brass U.S.A. standard sieves E-11 (0.05 m depth and 0.20 m in diameter) according to the following procedure. Sieves were nested in decreasing order of size and a sieve pan was placed at the bottom. Then a moderate amount of catalyst sample was put into the sieve placed in the top of the arrangement (170 mesh). Subsequently, the nested sieves were placed into the mechanical shaker operating at 300 strokes per minute and sieving procedure was lasted 30 minutes. During sieving, the side of the sieves was tapped to cause the particles to bounce, tumble or otherwise turn so as to present different orientations to the sieving surface.

Slurry reactor tests

Details of the reactors tests such as experimental set up, operating procedures and product quantification can be found elsewhere [42-44]. However, a brief description of experimental apparatus is given below.

Reactor tests were performed in a one cubic decimeter stirred tank slurry reactor (Autoclave Engineers). The feed gas flow rate was adjusted with a mass flow controller and passed through a series of oxygen removal, alumina and activated charcoal traps to remove trace impurities. After leaving the reactor, the exit gas passed through a series of high and low (ambient) pressure traps to condense liquid products. High molecular weight hydrocarbons (wax), withdrawn from the slurry reactor through a porous cylindrical sintered metal filter, and liquid products, collected in the high and low pressure traps, were analyzed by gas chromatography. Catalyst samples were withdrawn from the reactor at TOS= 0 hours (TOS= time on stream) and at the end of the run (EOR). After catalyst/wax separation, the PSD and morphology of wax-free catalyst samples were determined to assess their attrition properties.

Catalyst/wax separation

Catalyst/wax slurry was withdrawn from the STSR through a dipleg tube to a sampling cylinder, which was previously purged with nitrogen. Subsequently, the slurry was melted by heating the sampling cylinder and collected in a glass beaker. The slurry was diluted with a hot (~100ºC) mineral spirit solvent (Varsol). Catalyst was separated from the slurry by vacuum filtration using a glass-fritted funnel covered with a filter paper (Whatman No. 42) while adding hot solvent. This washing was repeated several times until the complete wax removal was achieved (see Figure 12). Finally, the excess solvent was evaporated and the wax-free catalyst was kept in a glass vial for PSD and SEM analyses.
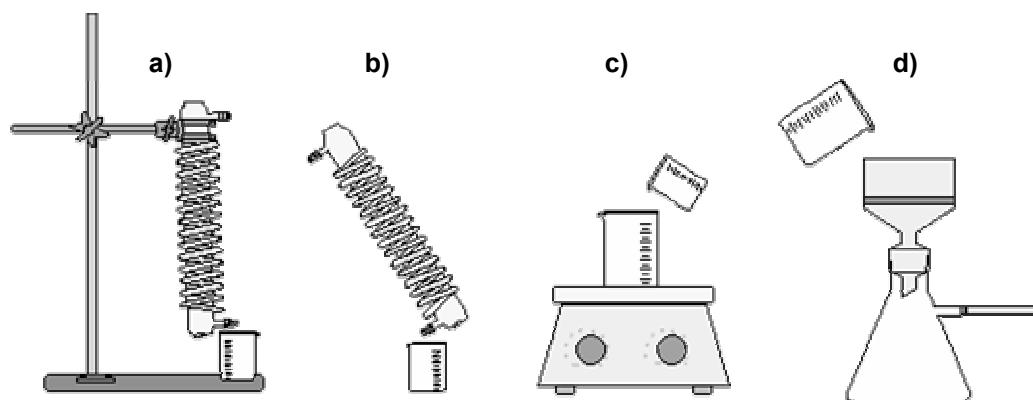
Figure 12. Catalyst/wax separation was accomplished by: (a) heating the sampling cylinder to melt the catalyst/wax mixture; (b) diluting it with hot (~100 ºC) mineral spirit solvent; (c) diluted mixture was then stirred and maintained at ~100ºC and; (d) repeatedly vacuum filtered to remove the solvent/wax mixture.

Morphological analysis: Scanning Electron Microscopy (SEM)

Samples submitted for SEM analyses can be usually examined with little specimen preparation. The first step is to collect a small amount of catalyst (few milligrams), which is assumed to be representative of the whole amount of catalyst. Then this sample was mounted for SEM examination according to the procedure described below.

Whenever it was needed, the catalyst sample was dried in a vacuum oven in order to remove impurities, which may interfere with the sample coating or the SEM examination. In order to prepare the catalyst sample, a double-stick adhesive carbon tape, previously mounted on SEM specimen stubs, was used. Then the catalyst particles were transferred to the carbon tape by a spatula. The excess of particles (loose particles) was removed by a gentle air stream since they might produce charging effects. Subsequently, SEM specimen was coated with an Au/Pd layer using a Hummer Sputter

Coater at 10 mA for 8 minutes (in a vacuum/He environment). Finally, SEM specimens were observed at different magnifications using a JEOL JSM-6400 Scanning Electron Microscope (see Figure 13) at an acceleration voltage of 15 kV and a working distance of 39 mm.
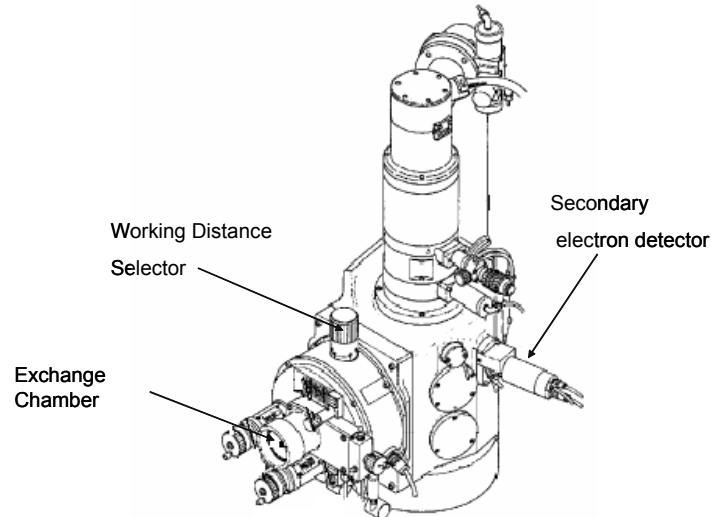
Figure 13. Schematic representation of JEOL JSM-6400 Scanning Electron Microscope. (From Bridges et al. [45]).

Particle size distribution (PSD): Coulter Counter Multisizer

PSD measurements were made in the Civil Engineering Department at TAMU, using a Coulter Counter Multisizer analyzer (see Figure 14), which employs the electrical sensing zone method to provide a particle size distribution analysis within a wide range of particle sizes. Each result is displayed graphically as a percentage of channel content, which can be selected to represent volume (weight), number (population) or surface area, in either differential or cumulative form. The measurable particle size range for this instrument is from about 0.4 μm to 1200 μm depending on the aperture tube selected. However, there is not a single aperture tube that can cover the complete range of particle sizes of interest. In order to overcome this drawback, a combination of aperture tubes

was used to cover the entire particle size range. For the samples used in this work, the aperture tubes sizes selected were 50 and 280 μm, which cover the particle size range from 1 to 168 μm.
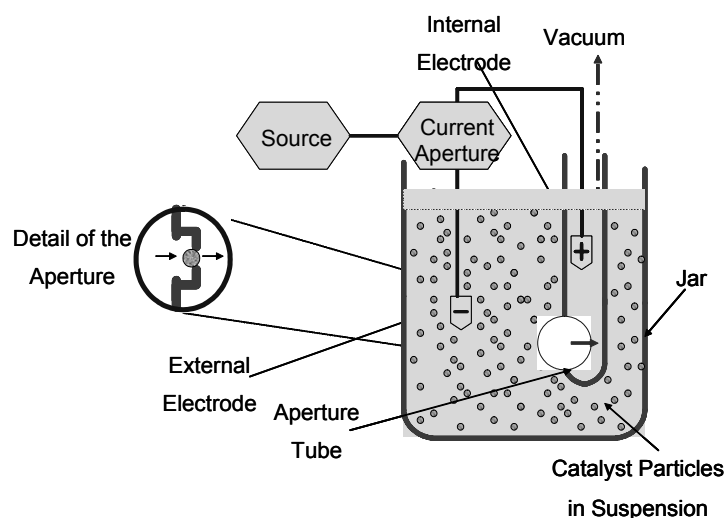
Figure 14. Schematics of the basic components of the Coulter Counter Multisizer.

Sample preparation

Raw samples were prepared using ~14 mg of catalyst powder in a glass vial (0.2 cm in diameter and 0.8 cm in height). Afterwards, 2-3 droplets of nonionic dispersant (Beckman-Coulter), type IB, were added to the vial in order to wet all the powder. Subsequently, 20 ml of electrolyte solution (Isoton II from Beckman-Coulter) were added, and the vial was shaken gently until complete homogenization was achieved. Finally, 4 ml of this raw sample was diluted with Isoton II solution in a sample jar containing electrolyte solution to 250 ml, and this sample was used for PSD measurements.

PSD measurement procedure and data collection

In order to cover the whole range of particle sizes for the measurements done in this work, two different aperture tubes sizes were used, 50 and 280 μm (measurable range: 1-168 μm). The procedure used to obtain PSD of catalyst samples is described below.

Diluted catalyst samples were mixed gently to get a homogeneous suspension and simultaneously, the samples were analyzed with the Coulter® Counter Multisizer, using an aperture tube of 280 μm. For all samples, at least three multiple measurements were performed, and the final results are reported as average values. These average values only cover the particle size range of 6-168 μm. Therefore, the catalyst samples were also analyzed using an aperture tube of 50 μm in order to cover the particle size range of 1-30 μm. For this second set of measurements, the catalyst samples in suspension were kept unmixed for about 30 minutes to let the bigger particles settle down and prevent them from blocking the aperture tube. Then, as done with the aperture tube of 280 μm, the samples were analyzed and the results of three multiple measurements for each sample were averaged. Finally, the results obtained from two aperture tubes (i.e. 50 and 280 μm) were combined using the Coulter® Multisizer AccuComp® software v. 1.19 to get the PSD measurement result (of number distributions and/or volume distributions) covering the whole particle size range for the sample analyzed.

Table 7 shows results obtained for catalyst DPS3616. The volume moment diameters from multiple measurements using aperture tubes of 280 and 50 μm were 47.10 ± 4.1 and 3.80 ± 0.1 respectively. This table also shows the average volume moment diameter for the catalyst sample obtained by combining results from the two aperture tubes. Figures 15-19 show differential distributions (volume %) of multiple measurements (Figures 15 and 17), average distributions (Figures 16 and 18) and combined distribution (Figure 19) using both 280 and 50 μm aperture tubes.

Table 7. Volume mean diameter ($d_{4,3}$) obtained from three measurements with DPS3616 catalyst

Aperture Tube Size	Volume moment diameter ($d_{4,3}$) ± S.D., μm
280 μm	47.10 ± 4.1
50 μm	3.80 ± 0.1
Multi Tube Overlap (280 + 50 μm)	45.4

Particle size distributions for attrition studies are usually plotted as volume distributions (see Figures 15-19), but it is a common practice to represent the whole distribution by mean or average diameter. Two types of average particle size diameters are used in this work, the so-called *Sauter mean diameter* (typically used to represent particle sizing in spray drying technique) and the *volume moment*. The latter was used previously in attrition studies of iron F-T catalysts [15-17, 26].

The Sauter mean diameter, d_{SV} ($d_{3,2}$), can be calculated by:

$$d_{SV} = d_{3,2} = \frac{\sum_1^i d_i^3 N_i}{\sum_1^i d_i^2 N_i} \quad \text{..............................} (10)$$

Where, d_i is the diameter of the particle i, and N_i is the number of particles with size d_i.

The volume moment, d_{VM} ($d_{4,3}$), can be calculated by:

$$d_{WM} = d_{VM} = d_{4,3} = \frac{\sum_1^i d_i^4 N_i}{\sum_1^i d_i^3 N_i} \quad \text{...........................} (11)$$

Where, d_{WM} is the weight moment diameter, and N_i is the number of particles having the diameter d_i.
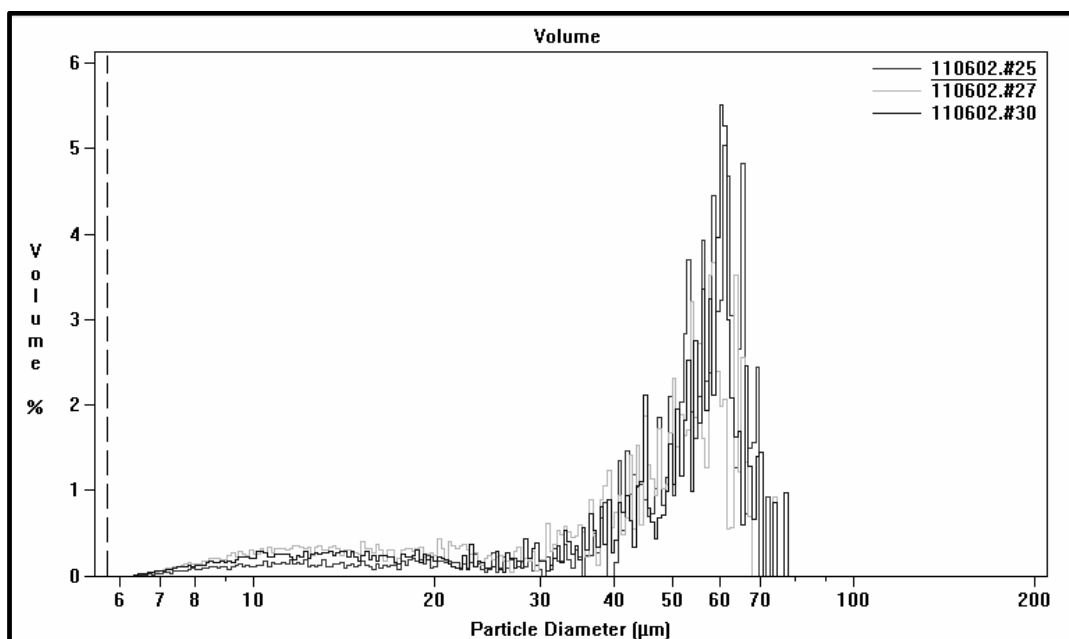
Figure 15. Superimposed distributions (from volume % distribution) for 3 multiple measurements for the catalyst DPS3616 using an aperture tube of 280 μm.
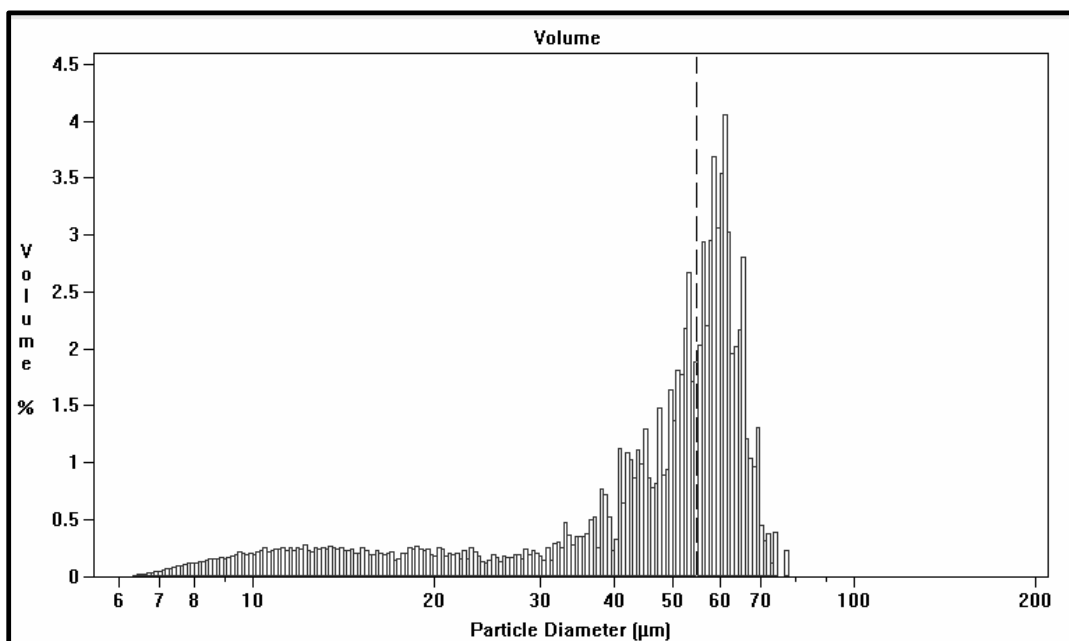
Figure 16. Average differential distribution (from volume % distribution) for the catalyst DPS3616 using an aperture tube of 280 μm.
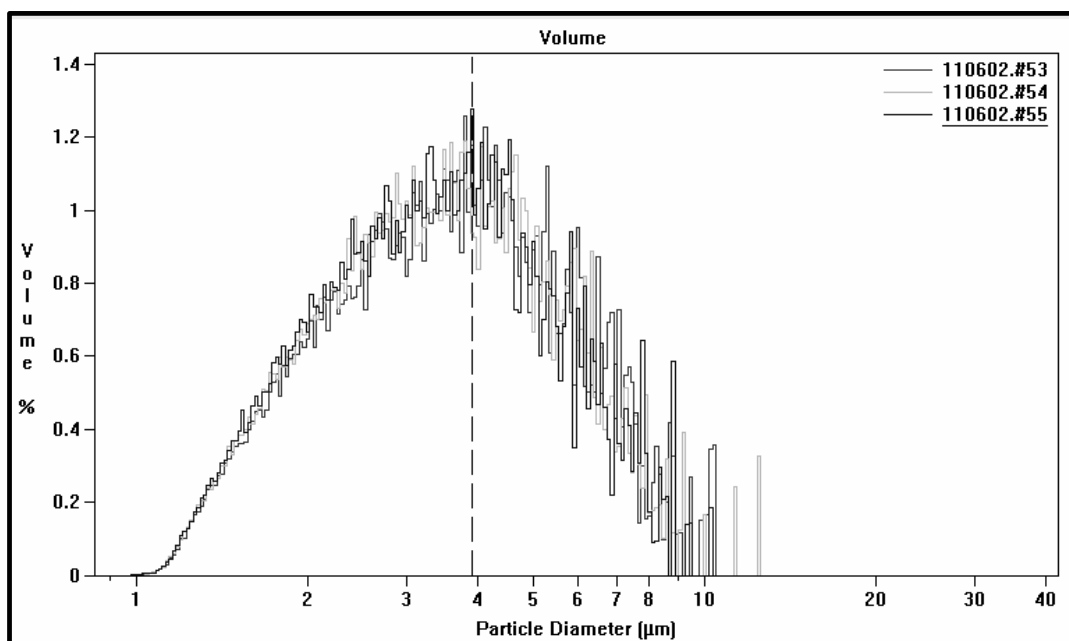
Figure 17. Superimposed distributions (volume %) for 3 multiple measurements for the catalyst DPS3616 using an aperture tube of 50 μm.
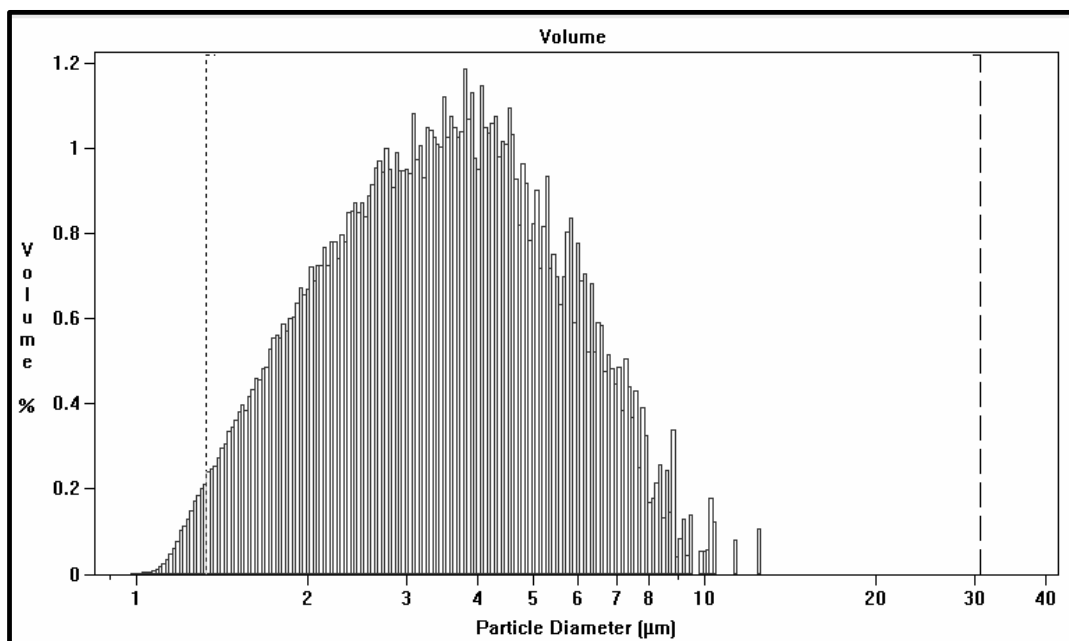
Figure 18. Average differential distribution (volume %) for the catalyst DPS3616 using an aperture tube of 50 μm.
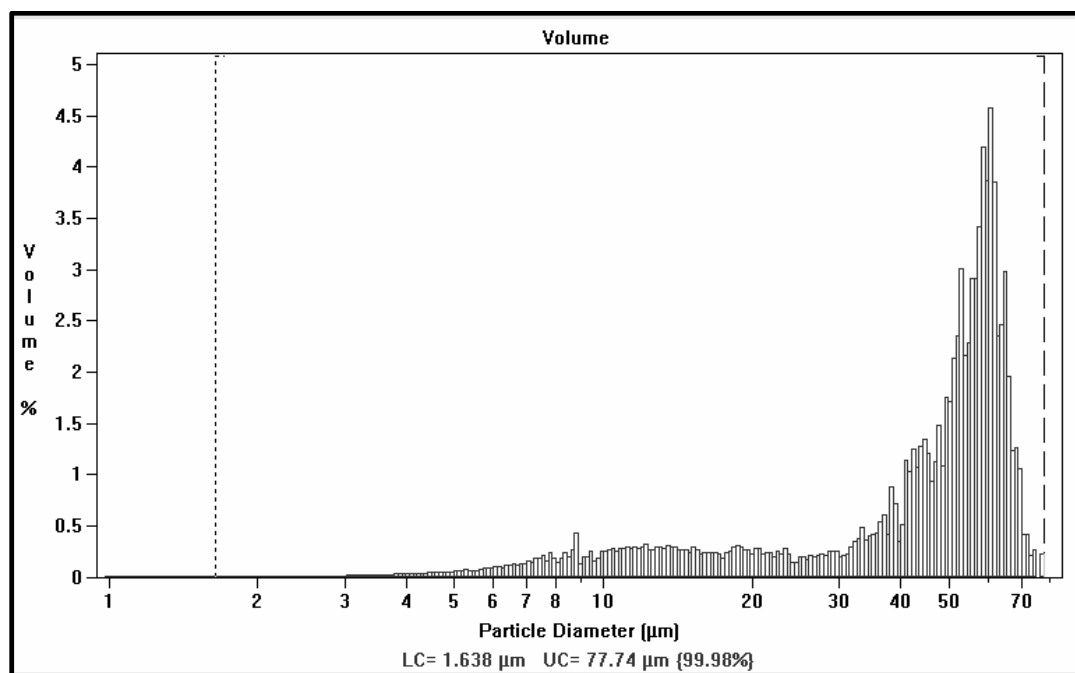
Figure 19. Overlapped distribution obtained from average results using two different aperture tubes (280 and 50 μm) for the catalyst DPS3616.

RESULTS

Catalyst synthesis and spray drying

Catalysts synthesized at TAMU and HU are listed in Table 7, together with information on the preparation procedure employed. Catalysts HU2061, HU1112 and HU3471 were prepared at HU as part of their on going research program supported by DOE. These catalysts were tested in the STSR at TAMU to evaluate their catalytic performance and attrition resistance. Commercial Ruhrchemie catalyst (CC3291) was also tested in the STSR at TAMU to assess its attrition resistance under F-T reaction conditions.

Table 7. Catalyst compositions and preparation methods employed

No.	Catalyst ID	Composition 100 Fe/x Cu/y K/z SiO$_2$	Silica Source	Spray Dried	Potassium Addition
1	**HU2061***	5 /4.2/11	TEOS	Yes	Wet Slurry
2	**HU1112***	3/4/16	TEOS	Yes	Wet Slurry
3	**HU3471***	5/4.2/1.1	Binder	Yes	Wet Slurry
4	**CC3291***	5/4.2/25	K$_2$SiO$_3$	No	Wet Slurry
6	**DPS5624-2***	5/6/24	K$_2$SiO$_3$	Yes	I.W.I. (before spray drying)
7	**DPS3616***	3/5/16 + 3 wt.% of silica binder	K$_2$SiO$_3$ + Bindzil 30/360	Yes	I.W.I. (before spray drying)
8	WPS3516-1	3/5/16 + 3 wt.% of silica binder	K$_2$SiO$_3$ + Bindzil 30/360	Yes	Drop-wise (wet slurry)
9	WPS3516-2			Yes	Drop-wise (wet slurry)
10	WPS3516-3			Yes	Drop-wise (wet slurry)
11	**PPS3516-1***	3/5/16	K$_2$SiO$_3$	No	Drop-wise (wet slurry)
12	WPS3516-4	3/5/16	K$_2$SiO$_3$	Yes	I.W.I. (after spray drying)
13	PPS3516-2	3/5/16	3/5/16	No	I.W.I.
14	**WCS3516-1***	3/5/16	Colloidal Silica	Yes	I.W.I. (after spray drying)
15	WCS3516-2			Yes	Drop-wise (wet slurry)
16	**WTO3516-1***	3/5/16	TEOS	Yes	I.W.I. (after spray drying)
17	WTO3516-2			Yes	Drop-wise (wet slurry)

* Catalysts in bold were used in slurry reactor tests at TAMU.

Precipitated catalyst precursors for the catalysts series DPS5624 and DPS3616 were synthesized previously at TAMU during DOE Contract DE-AC22-94PC93069 [21]. These two catalysts (100 Fe/5 Cu/6 K/24 SiO_2 – batch 5, and 100 Fe/3 Cu/4 K/16 SiO_2 – batch 3) were sieved and particles which passed through 325-mesh sieve (less than 45 μm in diameter) were collected, reduced in size (see Figure 20) and reslurried as described above. The resulting slurries were spray dried at TAMU. Catalyst DPS5624-2 was spray dried at 250°C in a large APV Anhydro spray dryer, whereas catalyst DPS3616 was mixed with silica binder – Bindzil 30/360 (3 wt. % SiO_2 of the total mass of the catalyst) prior to spray drying in the APV Anhydro Lab. S1 spray dryer at 210 °C.

Catalysts WPS3516-1 to -3 and PPS3516-1 catalyst were prepared from the same wet Fe/Cu/K/SiO_2 precursor. A portion of this precursor was vacuum-dried and then crushed to reduce the particle size of the catalyst (PPS3516-1), whereas silica binder (3 wt. % SiO_2 of the estimated total mass of dried catalyst) was added to the remaining precursor. Subsequently, the Fe/Cu/K/SiO_2 wet precursor was divided into three fractions, two of them (WPS3516-1 and -2) were spray dried in the APV Anhydro Lab. S1 spray dryer at 215 and 205 ºC respectively. The third fraction (WPS3516-3) was spray dried at 205 °C in the large APV Anhydro spray dryer. On the other hand, catalysts WPS3516-4 and PP3516-2 were also prepared from the same wet Fe/Cu/SiO_2 precursor. Once again, the catalyst precursor was divided into two fractions. One of them was vacuum-dried and then the potassium promoter was added by I.W.I. method (PP3516-2). The remaining portion of the precursor was spray dried in an APV Anhydro Lab. S1 spray dryer at 215 ºC. Subsequently, this fraction was impregnated with potassium by I.W.I. method (WPS3516-4).

Catalysts WCS3516-1 and -2 were prepared from the same Fe/Cu/SiO_2 precursor (using colloidal silica as the silica source), which was then divided into two fractions. One fraction was spray dried after addition of potassium promoter (WCS3516-2), whereas the remainder was first spray dried and potassium promoter was added later by I.W.I.

method (WCS3516-1). Both fractions were spray at 210 ºC in the APV Anhydro Lab. S1 spray drier. Methods of potassium addition for catalysts WTO3516-1 and -2 were the same as for catalysts WCS3516-1 and -2 respectively, but the silica source for WTO3516 catalysts was tetraethyl orthosilicate.
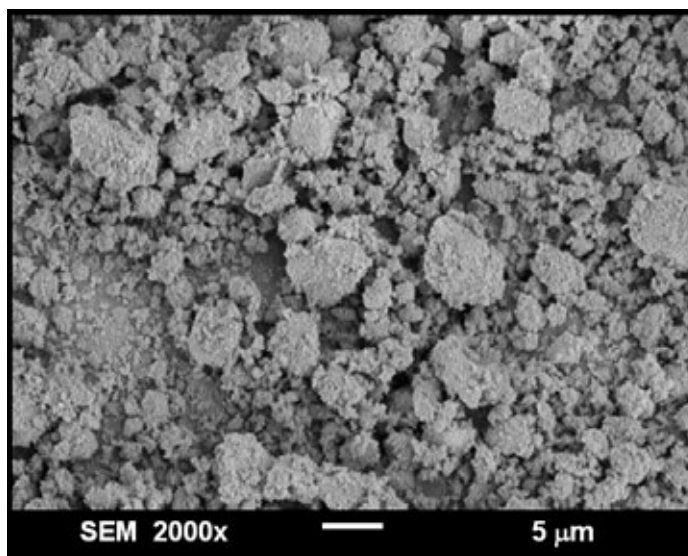
Figure 20. SEM micrograph of precipitated catalyst 100 Fe/5 Cu/6 K/24 SiO_2 after being crushed in a tumbler. Larger particles are around 5 μm in diameter, whereas smaller ones are less than 1 μm in diameter.

Morphology of spray dried materials

Morphology of spray dried model systems

Several spray-drying experiments were made using two model systems, iron oxide and iron oxide/silica binder. The goal of these experiments was to gain experience with the operation of the spray dryer, and to study the effect of operational parameters and feed properties on morphology and particle size of spray dried materials. Results of these experiments are summarized below.

Spray drying of iron oxide powders

In the first set of experiments, iron oxide (Alfa Aesar) with average diameter below 5 μm was mixed with distilled/deionized water to prepare 20-30 wt. % slurries. Subsequently, these slurries were spray dried at 220-300 ºC in the APV Anhydro Lab. S1 spray dryer. Representative SEM micrographs of collected spray-dried materials are shown in Figures 21 and 22. Pure iron oxide did not agglomerate well, regardless of the operating conditions. In another set of experiments, iron oxide (Bayferrox 105M from Bayer) with average diameter of 0.25 μm was used to prepare slurries with similar slurry concentrations. Figure 23 shows a SEM micrograph of spray dried Bayferrox 105M (20 wt. % slurry and 220ºC). Once again, the resulting powder consisted of small irregularly shaped agglomerates. Particle size and morphology were not markedly dependent on operational parameters or slurry properties (results not shown).
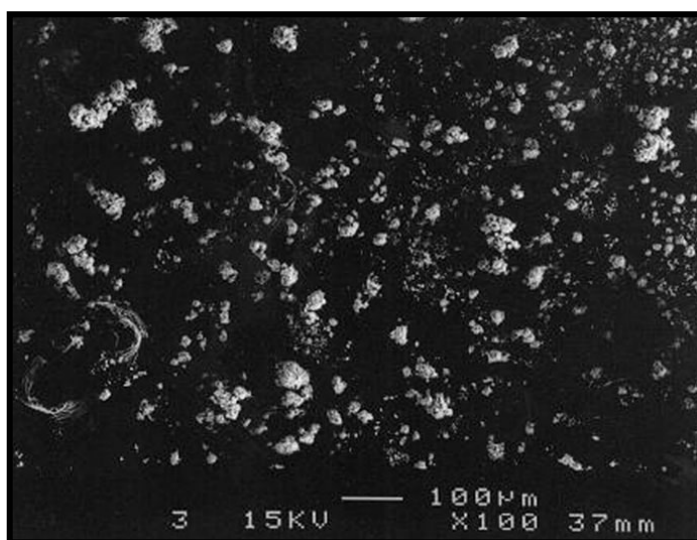
Figure 21. SEM image of spray dried Fe_2O_3 from Alfa Aesar (at 300 ºC and 20 wt. % slurry). The resulting powder consisted of small irregularly shaped agglomerates.
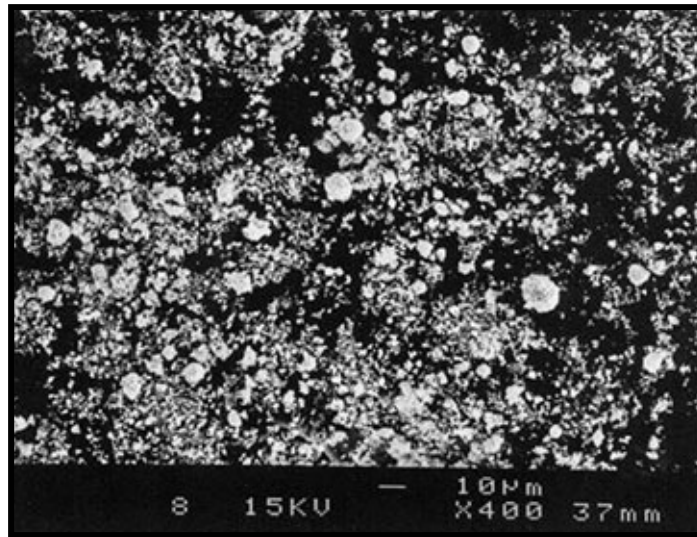
Figure 22. SEM image of spray dried Fe_2O_3 from Alfa Aesar (at 300 ºC and 30 wt. % slurry). Occasional semi-spherical agglomerates can be observed. However, most of the particles did not agglomerate.
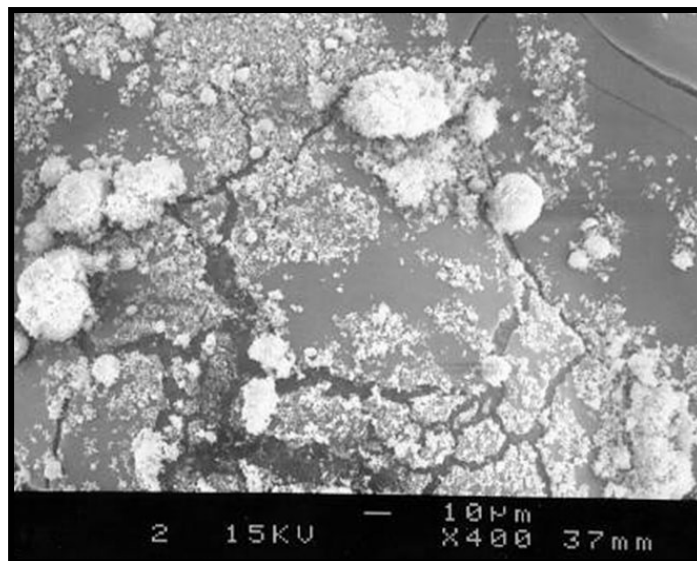
Figure 23. SEM image of spray dried Fe_2O_3 –Bayferrox– (at 220 ºC and 20 wt. % slurry). Iron oxide formed some irregular agglomerates. However, most of the material did not agglomerate.

Spray drying of iron oxide/colloidal silica model systems

In another set of experiments, Bayferrox 105M iron oxide powder was mixed with distilled/deionized water and commercial binder silica (Bindzil 30/360) in order to form 20-40 wt. % slurries, which were then spray dried at 200-300 ºC. The amount of binder silica added was chosen to give 11 wt. % of silica, based on the total weight of solid. Addition of binder silica resulted in formation of particle agglomerates with smooth surfaces. However, most of the particles showed a dimpled morphology (Figure 24). Modification of slurry feed properties resulted in substantial reduction of dimpled particles. Figure 25 shows the presence of largely spherical agglomerates with smooth external surface. Particle size was not markedly dependent on operating conditions.
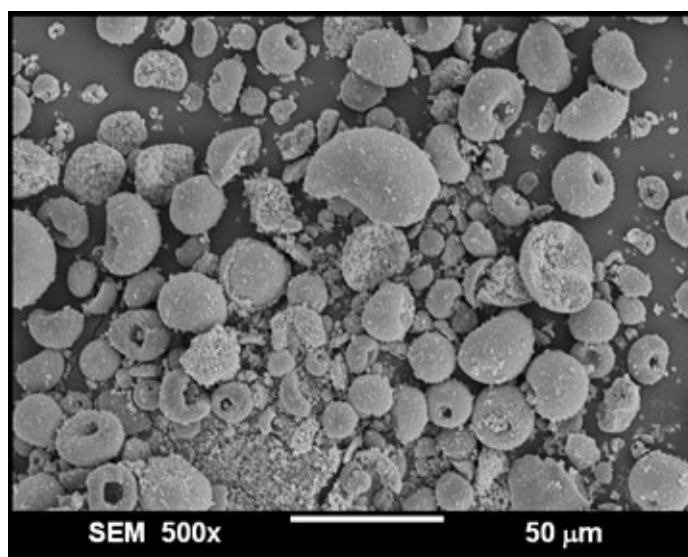
Figure 24. SEM micrograph of spray dried Bayferrox/binder silica (at 210 ºC from 40 wt. % slurry). Agglomeration of primary particles was considerably improved relative to spray dried pure iron oxide. However, a fairly large fraction was irregularly shaped (dimpled particles).
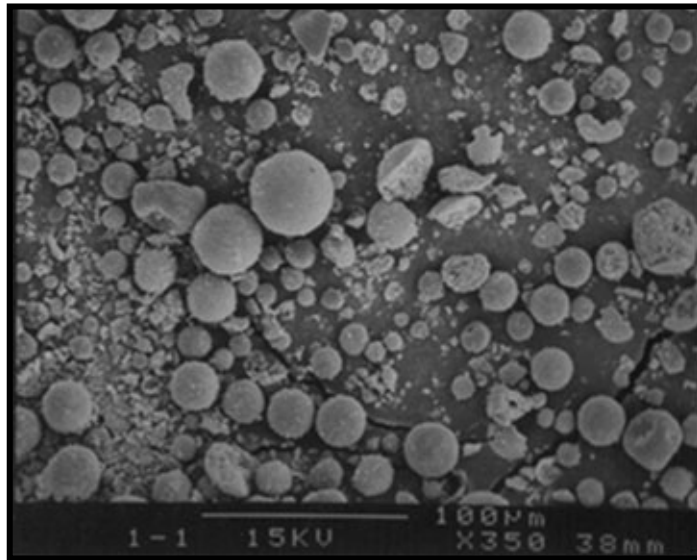
Figure 25. SEM image of spray dried Bayferrox/binder silica. Addition of silica binder and modification of slurry feed properties resulted in formation of largely spherical agglomerates with smooth external surface.

Morphological results obtained from experimental runs using model systems (i.e. pure Fe_2O_3 and Fe_2O_3/binder silica) showed that spray drying of pure iron oxide does not form agglomerates within a wide range of operating conditions employed. On the other hand, addition of silica binder resulted in marked improvement in agglomeration of primary particles. Morphology of these agglomerates exhibited dependence on feed slurry properties. Particle size distribution and particle morphology of both pure Fe_2O_3 and Fe_2O_3/binder silica systems did not vary much with slurry concentration and/or operating conditions (i.e. feed flow rate, temperature, atomizer type and/or rotational speed).

Morphology of spray dried iron F-T catalysts

Spray dried catalysts prepared at Hampton University

SEM micrographs of uncalcined and unsieved spray dried catalysts (as received samples) prepared at Hampton University are shown in Figures 26-28. Particle size distribution of spray dried 100 Fe/5 Cu/4.2 K/11 SiO_2 catalyst (HU2061) is very broad and most of the particles are irregularly shaped with some of them having plate-like morphologies (Figure 26). Smaller particles (5-10 μm) are nearly spherical, but with rough surfaces.

Most of particles of spray-dried 100 Fe/5 Cu/4.2 K/1.1 SiO_2 catalyst (HU3471) are spherical (Figure 27), but their external surfaces are relatively rough. Particle size distribution for this catalyst is also very broad. Figure 28 shows a micrograph of 100 Fe/3 Cu/4 K/16 SiO_2 catalyst (HU1112). This catalyst exhibits morphological features and particle size distribution similar to the ones found for catalyst HU3471.
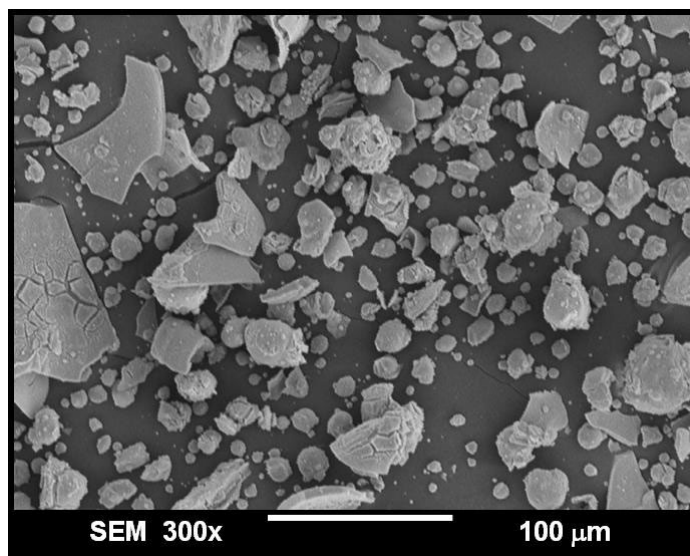
Figure 26. SEM image of spray dried HU2061 catalyst (No. 1 in Table 7). Its particle size distribution is very broad. Smaller particles (5-10 μm) are nearly spherical, whereas larger particles are of irregular shape, including some platelet like particles.
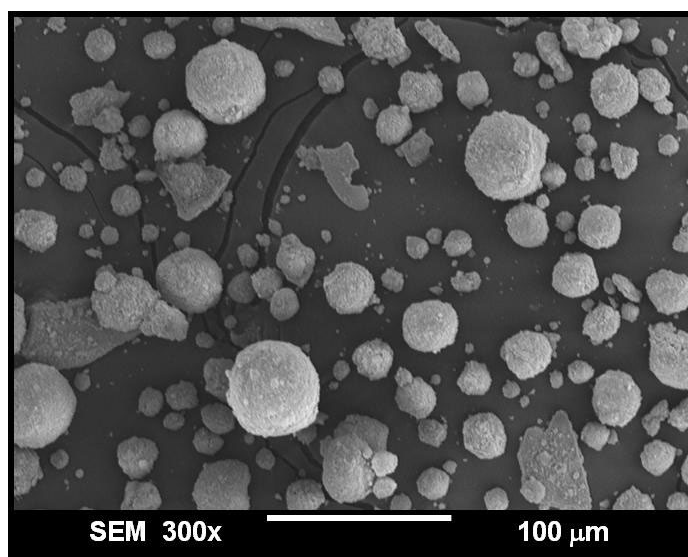
Figure 27. SEM image of spray dried HU3471 catalyst (No. 3 in Table 7). Majority of particles are nearly spherical, but external surfaces are relatively rough and smaller particles are attached to the surface.
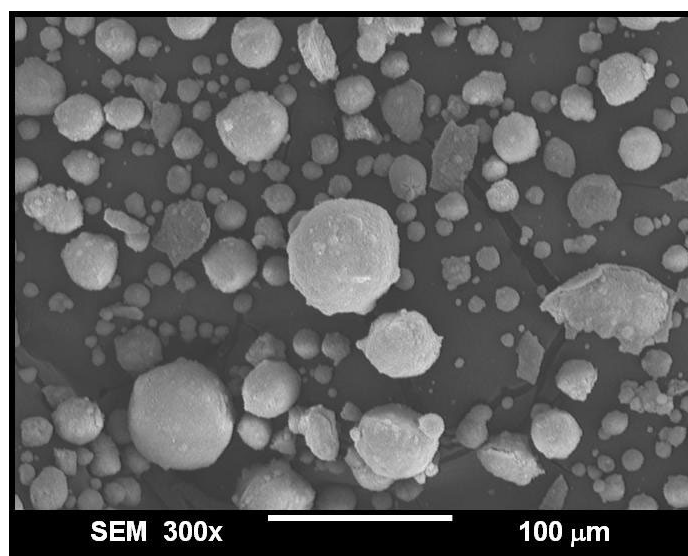
Figure 28. SEM image of spray dried HU1112 catalyst (No. 2 in Table 7). Majority of particles are nearly spherical, but external surfaces are relatively rough and smaller particles are attached to the surface.

Catalysts prepared at TAMU

SEM micrographs of as spray dried catalysts synthesized at TAMU are shown in Figures 29-33. Catalysts prepared from vacuum dried precursors (Figures 29 and 30) have a significant number of irregularly shaped particles (large particles), whereas smaller particles are nearly spherical. Catalyst 100 Fe/3 Cu/6 K/16 SiO_2 (Figure 29) containing precipitated silica plus 3 wt. % of SiO_2 from Bindzil 30/360 (DPS3616) was spray dried in the APV Anhydro Lab. S1 spray dryer (1.1 m chamber diameter). Particle size for this catalyst is smaller in comparison to the catalyst DPS5624-2 (100 Fe/5 Cu/6 K/24 SiO_2), which was spray dried in the large APV Anhydro spray dryer (2.1 m chamber diameter). SEM micrograph of this catalyst (Figure 30) shows the presence of large irregularly shaped particles with smooth surfaces. From these micrographic results it is obvious that catalysts, which were spray dried from vacuum dried precursors do not form a large fraction of spherical particles.
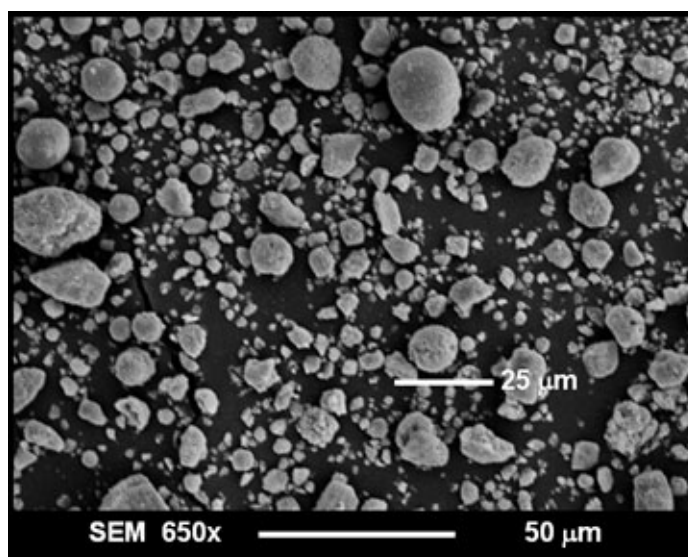
Figure 29. SEM micrograph of as spray dried catalyst DPS3616 prepared from vacuum dried precursors (No. 7 in Table 7). Larger particles are irregularly shaped; whereas smaller ones are nearly spherical.
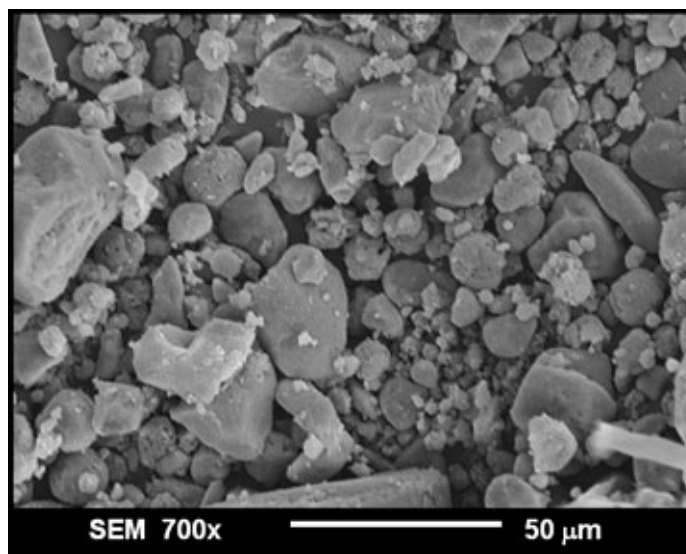
Figure 30. SEM micrograph of as spray dried catalyst DPS5624-2 prepared at TAMU from vacuum dried precursors (No. 6 in Table 7). This sample has a significant number of irregularly shaped particles (large particles) whereas smaller particles are nearly spherical.

Representative SEM micrographs of spray-dried catalyst from wet precursors are shown in Figures 31 and 32. Catalysts prepared from wet precursors (Nos. 8-10, 12 and 14-17 in Table 7) have excellent sphericity and smooth surfaces. All these catalysts (except No. 10) were prepared in the APV Anhydro Lab. S1 spray dryer. The observed morphology of these spray-dried catalysts makes them suitable for use in slurry reactors. Sphericity is important for maintaining catalyst's mechanical integrity during F-T synthesis in a slurry reactor. Figures 31 and 32 show SEM micrographs of catalysts 100 Fe/3 Cu/5 K/16 SiO_2 (SiO_2 from potassium silicate) + 3 wt. % of SiO_2 from binder silica (Bindzil 30/360). These figures demonstrate that sphericity of spray-dried catalysts can be controlled through the use of appropriate operating conditions. Operation outside the range of optimal parameters leads to formation of dimpled particles (Figure 31), whereas selection of a proper set of parameters leads to formation of particles having excellent sphericity (Figure 32).

Spray dried catalysts from wet precursors exhibited broad particle size distributions, ranging from 5 to about 40 μm, regardless of the source of silica used (i.e. potassium silicate, TEOS or colloidal silica). It should be noted that SEM micrographs have bias toward smaller particles, since larger particles are preferentially blown away during sample preparation.

Figure 33 shows a SEM micrograph of PPS3516-1 catalyst (precipitated catalyst – non-spray dried). Precipitated catalysts have irregularly shaped particles with sharp edges. There is concern that non-spherical catalysts may not be attrition resistant during testing in slurry reactors.
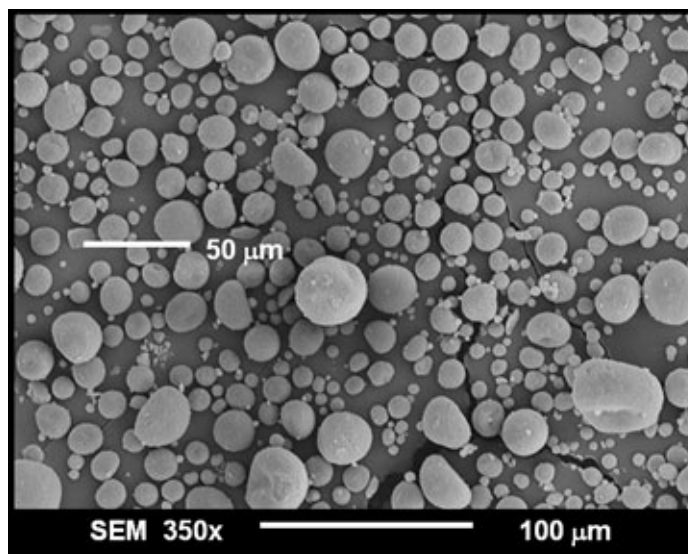
Figure 31. SEM micrograph of as spray dried catalyst WPS3516-1 prepared from wet slurries (No. 8 in Table 8). Catalyst particles have smooth surfaces and semi-spherical shape. However, some of them exhibit a dimpled morphology.
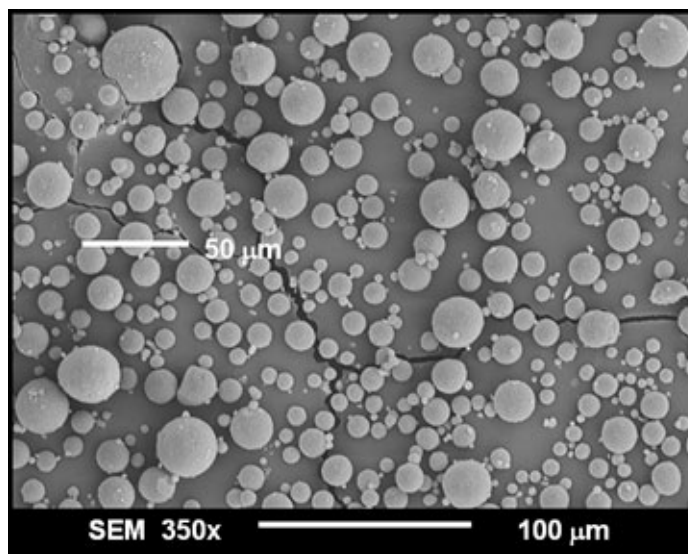
Figure 32. SEM micrograph of as spray dried catalyst WPS3516-2 prepared from wet slurries (No. 9 in Table 7). Catalyst particles exhibit excellent sphericity with smooth surfaces.
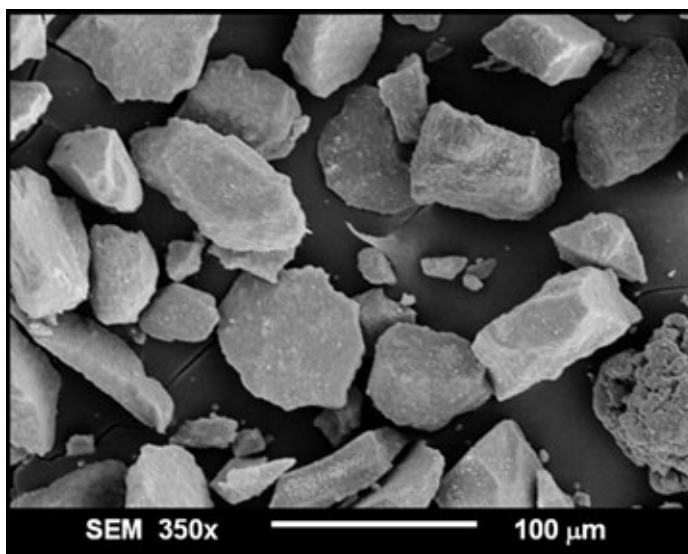
Figure 33. SEM micrograph of catalyst PPS3516-1 prepared from wet slurries (No. 11 in Table 7). Catalyst particles are irregularly shaped with smooth surfaces.

Sieving results of spray dried catalysts

Spray dried catalysts prepared at HU and TAMU were sieved in order to classify each sample according to selected particle size ranges. Catalysts were sieved in a mechanical shaker for 30 minutes. Table 8 lists sieving results of several spray-dried catalysts used in this work. Results show that HU1112 catalyst contains 21.0 wt. % of particles between 45 and 90 μm, whereas 61.0 wt. % of this catalyst is below 45 μm. On the other hand, spray dried catalysts prepared at TAMU consist basically of particles smaller than 45 μm regardless of the spray dryer unit employed. TAMU catalysts were collected from the cyclone separator, and were not mixed with particles retained on the chamber walls of the spray drier.

Table 8. Sieving results of spray-dried catalysts

Catalyst ID	Sieved fractions, wt. %		
	< 45 μm	45-90 μm	> 90 μm
HU1112 [$]	61.0	21.0	17.9
WPS3516-3 [&]	99.20	0.80	0.00
WCS3516-1 [#]	99.4	0.4	0.2
WTO3516-1 [#]	99.1	0.8	0.1

[$] Spray dried at HU in a bench-scale Niro spray dryer (0.90 m in diameter and 1.8 m height).
[&] Spray dried at TAMU in the APV Anhydro (2.1 m in diameter and 2.4 m height).
[#] Spray dried at TAMU in the APV Anhydro Lab. S1 spray dryer (1.1 m in diameter and 2.4 m height).

Attrition behavior of TAMU and HU catalysts during STSR tests

Table 9 summarizes nine slurry reactor tests performed at TAMU during the period of this project that is supported by DOE under Grant No. DE-FG26-00NT40822. As it was stated previously, the goal of reactor tests was to evaluate catalytic performance of iron F-T catalysts synthesized at HU and TAMU under slurry reactor conditions. Additionally, these tests enable us to assess catalysts' attrition behavior under reaction conditions in the STSR. Analysis and discussion of catalytic performance results obtained during this project are beyond the scope of this thesis. Reaction conditions used

in each test are listed in Table 9, together with information on particle size of catalysts loaded into the reactor.

Table 9. Catalysts tested and reaction conditions

Catalyst ID/ Reactor Run	Catalyst 100 Fe/x Cu/y K/z SiO$_2$	Particle Size	Test Conditions [a]	Time Period
HU2061 SB-20601	5/4.2/11 (P)	Not determined	3.3 Nl/g-Fe/h, 2.1 MPa 5 Nl/g-Fe/h, 2.1 MPa	0-224 h; 334-380 h 224-*334 h**
HU1112 SB-11102	3/4/16 (P)	Not determined	3.9 Nl/g-Fe/h, 1.5 MPa 5.8 Nl/g-Fe/h, 2.2 MPa	0-210 h 215-*450 h**
HU3471 SB-34701	5/4.2/1.1 (B) SiO$_2$	Not determined	3.1 Nl/g-Fe/h, 2.1 MPa	0-*449 h**
CC3291 SB-32901	5/4.2/25 (P)	140-325 mesh	3.8 Nl/g-Fe/h, 1.5 MPa 2.3 Nl/g-Fe/h, 1.5 MPa 2.3 Nl/g-Fe/h, 2.2 MPa	0-209 h 210-325 h 326-*429 h**
PPS3516-1 SB-19102	3/5/16 (P)	170-325 mesh	4 Nl/g-Fe/h, 1.5 MPa 4 Nl/g-Fe/h, 2.2 MPa	0-197 h; 382-*500 h** 198-352 h
DPS5624-2 SB-16502	5/6/24 (P)	140-325 mesh	4 Nl/g-Fe/h, 1.5 MPa 5.8 Nl/g-Fe/h, 2.2 MPa	0-160 h 161-*295 h**
WCS3516-1 SB-30702	3/5/16 (B)	< 325 mesh	4 Nl/g-Fe/h, 1.5 MPa 6 Nl/g-Fe/h, 2.2 MPa	0-165 h; 292-*345 h** 166-291 h
WTO3516-1 SB-33802	3/5/16 (P)	< 325 mesh	4 Nl/g-Fe/h, 1.5 MPa 6 Nl/g-Fe/h, 2.2 MPa	0-178 h 179-*299 h**

[a] T= 260°C, H$_2$/CO = 0.67 in all tests.

(P) = Precipitated silica; (B) = binder silica.

* Period of exposure for each catalyst under slurry reactor conditions (*t*).

In order to evaluate the attrition strength of each catalyst listed above (Table 9), PSD measurements were performed before every reaction test (TOS= 0 h) and at the end of the run (TOS= *t* h). Samples collected at TOS= 0 h were withdrawn from the reactor before catalyst pretreatment and washed with Varsol to remove the initial slurry medium (Durasyn 164 oil). Samples collected at the end of the run, TOS= *t* h, were also withdrawn from the slurry reactor and washed with Varsol to get wax-free catalyst samples. PSD for each sample was obtained using the Coulter® Counter Multisizer. Subsequently, PSD data were used to calculate both the Sauter mean diameter and the volume moment diameter (see Table 10). Additionally, SEM micrographs were obtained to supplement results obtained from PSD measurements. Results for each catalyst are described in the following sections.

Table 10. Sauter mean diameter and volume moment diameter calculated from volume distributions data (from Coulter® Counter Multisizer PSD measurements)

Catalyst ID	TOS= 0 h		t^*, h	TOS= t h		% of change[#]	
	$d_{3,2}{}^{\&}$, µm	$d_{4,3}{}^{\$}$, µm		$d_{3,2}{}^{\&}$, µm	$d_{4,3}{}^{\$}$, µm	$\Delta d_{3,2}$	$\Delta d_{4,3}$
HU2061	48.0	52.8	380	6.2	18.1	87.0	65.7
HU1112	*40.1*	*49.6*	*450*	*27.0*	*46.8*	*32.7*	*5.6*
HU3471	*37.3*	*46.4*	*449*	*43.1*	*64.6*	*39.9*	*-2.2*
CC3291	34.1	46.9	429	25.8	40.2	24.3	14.3
PPS3516-1	47.1	53.1	500	30.8	43.2	34.6	18.6
DPS5624-2	48.3	57.3	295	33.1	48.1	31.5	16.1
WCS3516-1	20.6	24.1	345	19.2	22.8	6.8	5.4
WTO3516-1	*15.6*	*17.4*	*299*	*29.0*	*41.0*	*-85.9*	*-135.6*

$^{\&}$ $d_{3,2}$: Sauter mean diameter; $^{\$}d_{4,3}$: Volume moment diameter; * Time of exposure; $^{\#}$ % of change = $[(Y_{@TOS= 0 h} - Y_{@TOS= t h})/ (Y_{@TOS= 0 h})] * 100$; where Y= $d_{3,2}$ or $d_{4,3}$.
Italics are used when samples were washed several times.

Catalysts prepared at HU and the Ruhrchemie catalyst

Representative SEM micrographs and results from PSD measurements for catalysts prepared at HU and of the Ruhrchemie catalyst are shown in the figures on pp. 60-67. Figures 34 and 35 illustrate morphologies of the 100 Fe/5 Cu/4.2 K/11 (P) SiO$_2$ catalyst (HU2061) at TOS= 0 h and at the end of the run (TOS= 380 h). Catalyst at TOS= 0 h

consists of a mixture of irregularly shaped particles and some roughly spherical particles, which is probably due to the use of improper spray drying conditions. This was also observed with as received spray dried sample (Figure 26).
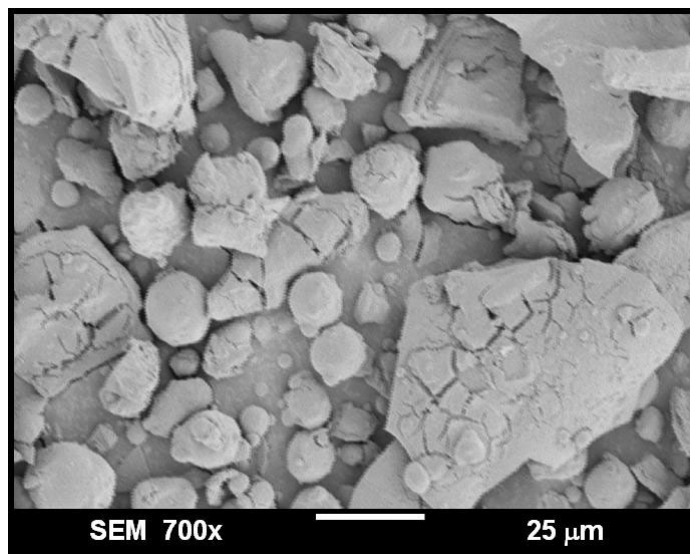
Figure 34. HU2061 catalyst withdrawn from the STSR (Run SB-20601) at TOS= 0 h. Larger particles are irregularly shaped (platelet like particles), whereas smaller ones are roughly spherical.

As suspected, HU2061 catalyst exhibited severe attrition by fracture of irregular particles after it was tested for 380 h in the STSR (run SB-20601) at 3.3-5 Nl/g-Fe/h, 260 ºC and 2.1 MPa. SEM micrograph of a sample collected at TOS= 380 h also shows that spherical particles eroded into primary particles below 5 μm in diameter (Figure 35). Table 10 shows that the volume moment diameter was reduced by 87.0 % relative to the sample at TOS= 0 h. Also, Figure 36 shows how the catalyst experienced a reduction in size after the reaction test. For instance, from Figure 36 it can be seen that at TOS= 0 h, 75 % of the particles (*x axis*) have a diameter larger than 49 μm (*y axis*), whereas after 380 h in the STSR, the reduction on the particle size can be observed since 75 % of the particles just have a diameter larger than 4.2 μm (see Figure 36).
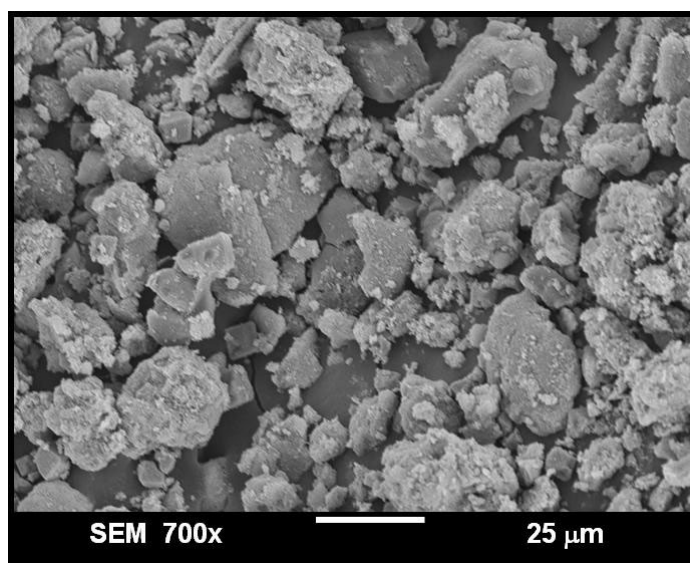
Figure 35. HU2061 used in run SB-20601 at TOS= 380 h. Catalyst particles suffered from fracture attrition. Also note the effect of erosion of spherical particles.
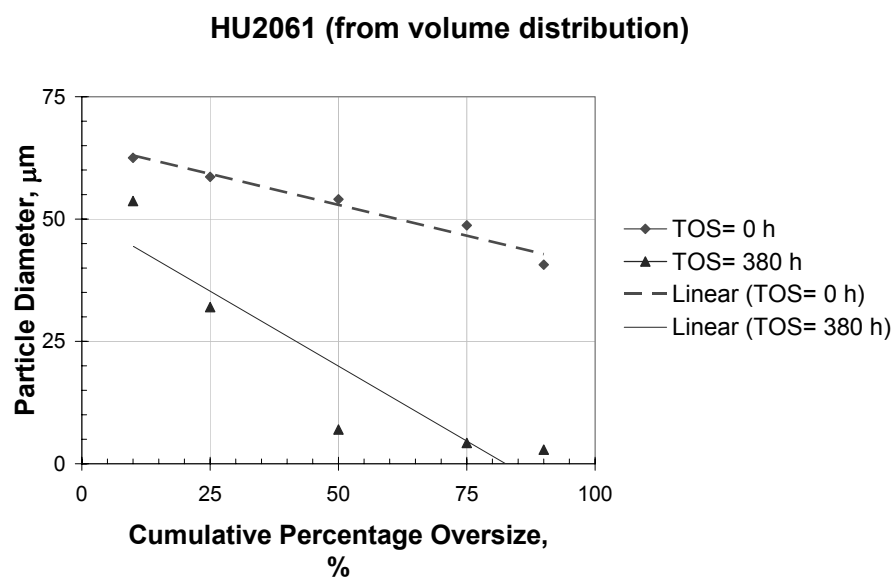
Figure 36. Percentiles (10, 25, 50, 75 and 90 %) obtained from volume distributions for the catalyst HU2061 (used in run SB-20601) at TOS= 0 h and TOS= 380 h.

Figures 37 and 38 show morphologies of 100 Fe/3 Cu/4 K/16 (P) SiO$_2$ catalyst (HU1112) at TOS= 0 h and at the end of the run (TOS= 450 h). Catalyst sample at TOS= 0 h is in the form of roughly spherical particles with some irregularities and uneven surfaces (Figure 37). PSD measurements show that after this catalyst was tested for 450 h in a STSR (run SB-11102) at 3.9-5.8 Nl/g-Fe/h, 260 ºC and 1.5-2.2 MPa it experienced a reduction of 32.7 % in its Sauter mean diameter and 3.6 % in its volume moment diameter (Table 10). Reduction in the volume moment diameter is not significant according to PSD results. SEM micrograph (Figure 38) shows that particle size was reduced during the STSR test. Also, the morphology of the catalyst changed considerably after the reaction test. Most of the spherical particles disappeared and there is a large number of irregularly shaped particles (~5 μm in diameter). Figure 39 shows that change in particle size distribution for this catalyst, formed mainly of spherical particles, is less pronounced than the one exhibited by the catalyst HU2061 (which is formed mainly of irregularly shaped particles).
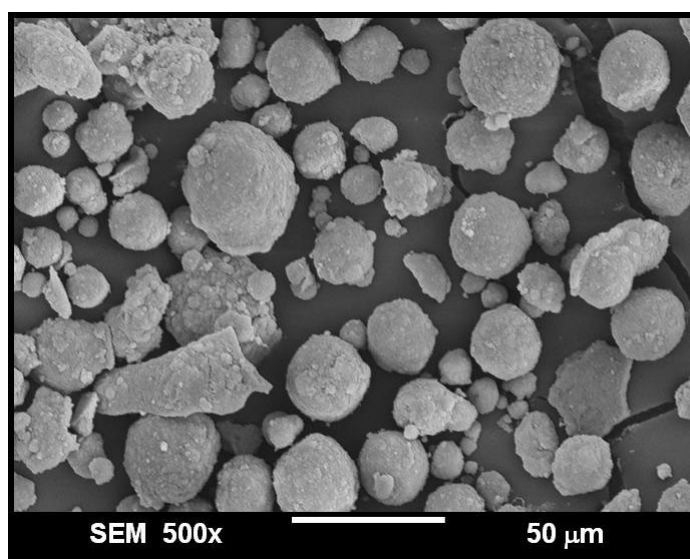
Figure 37. HU1112 catalyst withdrawn from the STSR (Run SB-11102) at TOS= 0 h. Most of the catalyst particles are spherical with uneven surfaces.
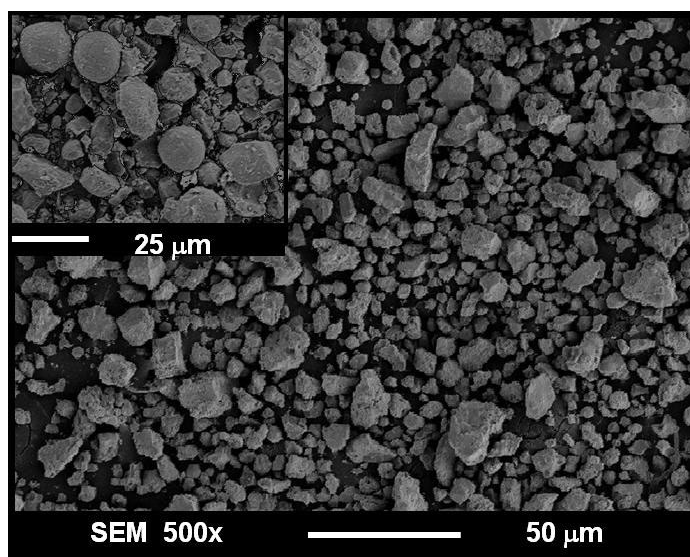
Figure 38. HU1112 catalyst withdrawn from the STSR (Run SB-11102) at TOS= 450 h and washed three times to get wax-free catalyst. Catalyst particles lost their sphericity; only a small fraction remained spherical after the test.
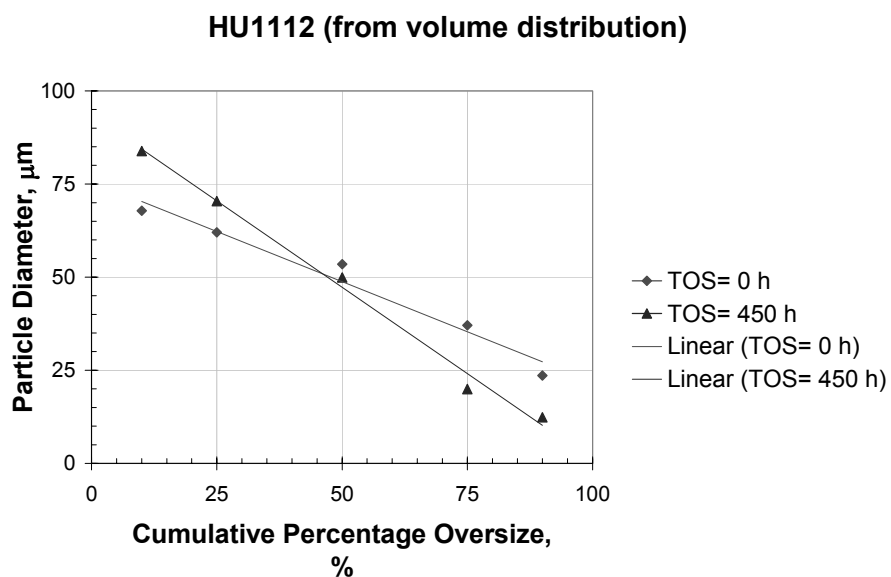
Figure 39. Percentiles (10, 25, 50, 75 and 90 %) obtained from volume distributions for the catalyst HU1112 (used in run SB-11102) at TOS= 0 h and TOS= 450 h.

Representative SEM images of 100 Fe/5 Cu/4.2 K/1.1 (B) SiO$_2$ catalyst (HU3471) at TOS= 0 h and at the end of the run (TOS= 449 h) are shown in Figures 40 and 41. The morphology of the sample at TOS= 0 h is very similar to that of HU1112 catalyst at TOS= 0 h. Most of particles are spherical with smaller agglomerates attached to their surfaces (Figure 40). On the other hand, the sample collected at TOS= 449 h has an irregular morphology since spherical particles practically disappeared after testing in the STSR (Run SB-34701) for 449 h at 3.1 Nl/g-Fe/h, 260 ºC and 2.1 MPa (Figure 41). After the test this catalyst experienced a 39.9 % reduction in its Sauter mean diameter (Table 10). In contrast, the volume moment diameter exhibited an increase of 2.2 %. Figure 42 shows an increase in the volume occupied by small particles after the reaction test. However, it is also obvious that there was an increase in the volume of larger particles. This strange behavior in the volume moment diameter change may be due the simultaneous and opposite effects of the fines generation by attrition, and agglomeration of particles due to presence of residual wax.
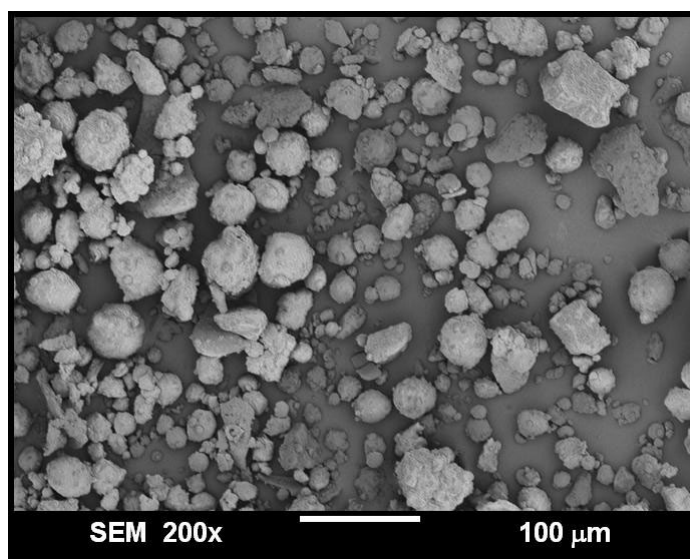
Figure 40. HU3471 catalyst withdrawn from the STSR (run SB-34701) at TOS= 0 h. Most of the catalyst particles are spherical with rough surfaces. Larger particles have small agglomerates attached to their surfaces.
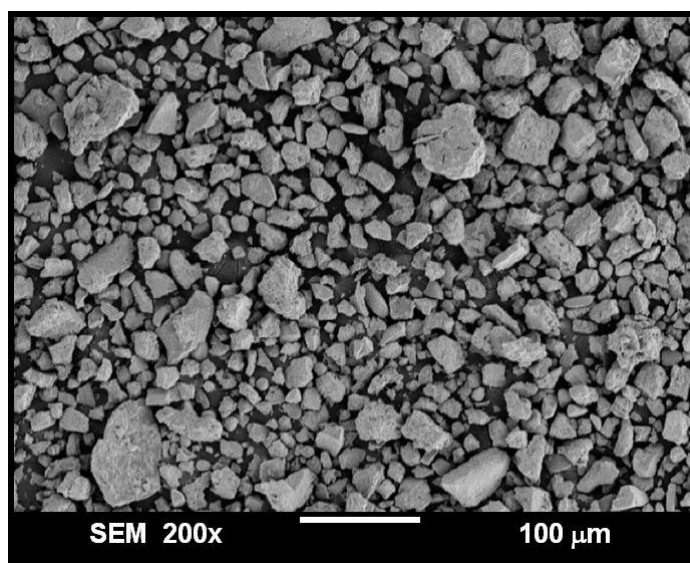
Figure 41. HU3471 catalyst withdrawn from the STSR (run SB-34701) at TOS= 449 h (after multiple washings to get free-wax catalyst samples). Most of the catalyst particles lost their sphericity after the reaction test.
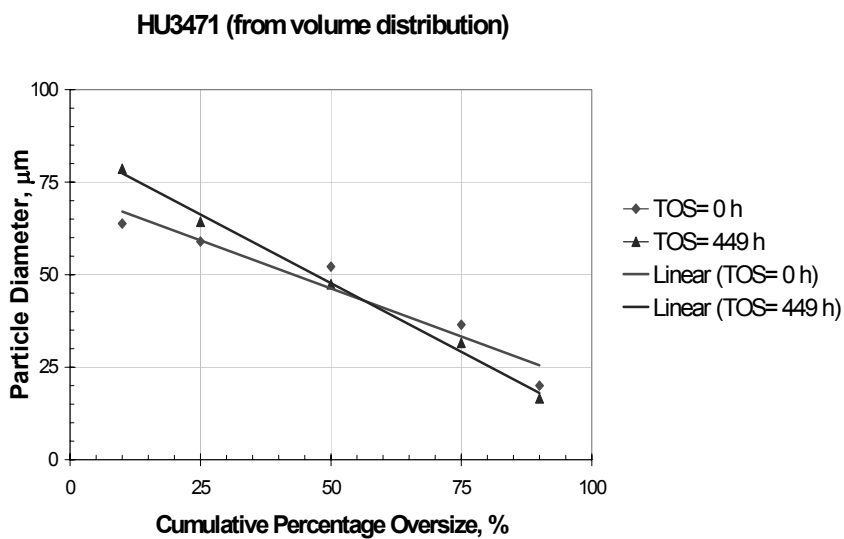
Figure 42. Percentiles (10, 25, 50, 75 and 90 %) obtained from volume distributions for the catalyst HU3471 (used in run SB-34701) at TOS= 0 h and TOS= 449 h.

Ruhrchemie catalyst (CC3291) was not prepared by spray drying technique. From Figure 43 it can be seen that the particle size distribution at TOS= 0 h for this catalyst is very similar to the one obtained after 429 hours of testing in the slurry reactor at 2.3-3.8 Nl/g-Fe/h, 260 ºC and 1.5-2.2 MPa (Run SB-32901). These results are supported by SEM micrographs shown in Figures 44 and 45. Catalyst morphologies before and after the reaction test are essentially the same. SEM images show that both catalyst samples are formed of irregularly shaped particles with smooth surfaces. It is hard to determine the attrition behavior of this catalyst from SEM micrographs. However, decrease in the Sauter mean diameter (24.3 %) and the volume moment diameter (14.3 %) indicate that fracture and/or erosion took place during the reaction test (Table 10).

CC3291 (from volume distribution)
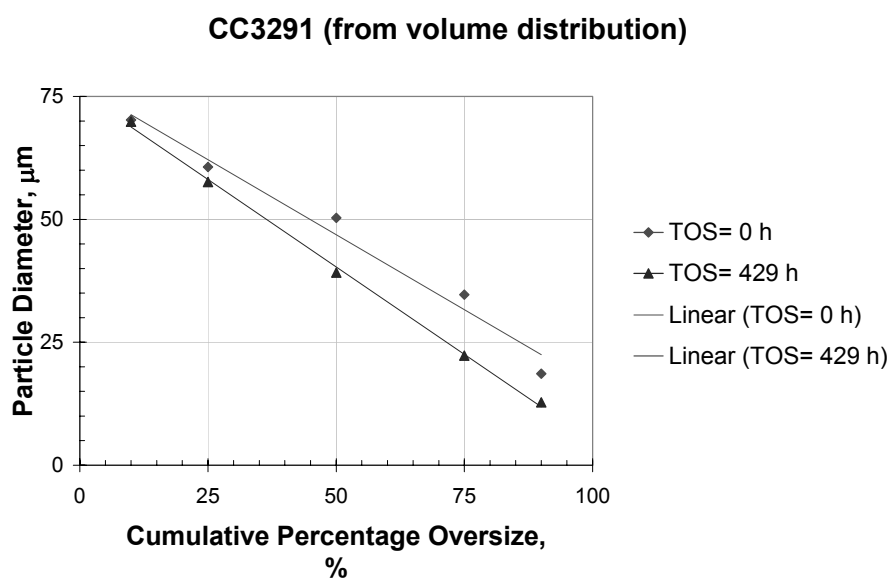
Figure 43. Percentiles (10, 25, 50, 75 and 90 %) obtained from volume distributions for the catalyst CC3291 (used in run SB-32901) at TOS= 0 h and TOS= 449 h.
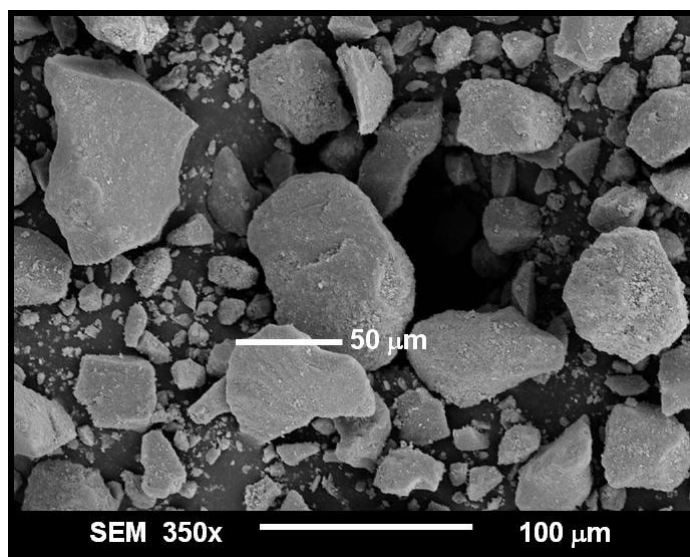
Figure 44. Ruhrchemie catalyst CC3291 at TOS= 0 h (used in run SB-32901). This catalyst is formed of irregularly shaped particles. SEM micrograph also shows that the sample has a wide particle size distribution even though this catalyst was sieved between 140 and 325 mesh (45-106 μm).
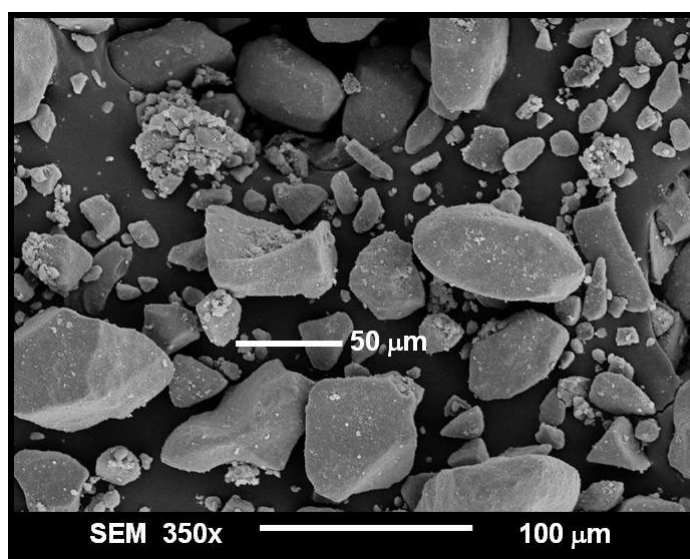
Figure 45. Ruhrchemie catalyst (CC3291) withdrawn from the STSR (run SB-32901) at TOS= 429 h. SEM micrograph does not show a significant change in the catalyst's morphology in relation to the catalyst's morphology before the reaction test.

Iron F-T catalysts prepared at TAMU

Representative SEM micrographs and results from particle sizing (using a Coulter[®] Counter Multisizer) of catalysts prepared at Texas A&M University are shown in the figures on pp. 68-77.

Precipitated catalysts (not spray dried)

SEM micrograph of 100 Fe/3 Cu/5 K/16 SiO$_2$ catalyst (PPS3516-1) collected at TOS= 0 h is shown in Figure 46. Most of particles are irregularly shaped with sharp edges and smooth surfaces. SEM micrograph (Figure 47) of the catalyst after 500 h of testing (at 4Nl/g-Fe/h, 260 ºC and 1.5-2.2 MPa) shows that some of the larger particles remained after the reaction test (SB-19102), but their edges are now rounded due to erosion effect. Fracture effect is also evident because some particles disintegrated into primary particles. The shift towards smaller particles after the reaction test is also evident from Figure 48. Sauter mean diameter and volume moment diameter decreased by 24.3 % and 14.3 %, respectively, during the STSR testing (Table 10).
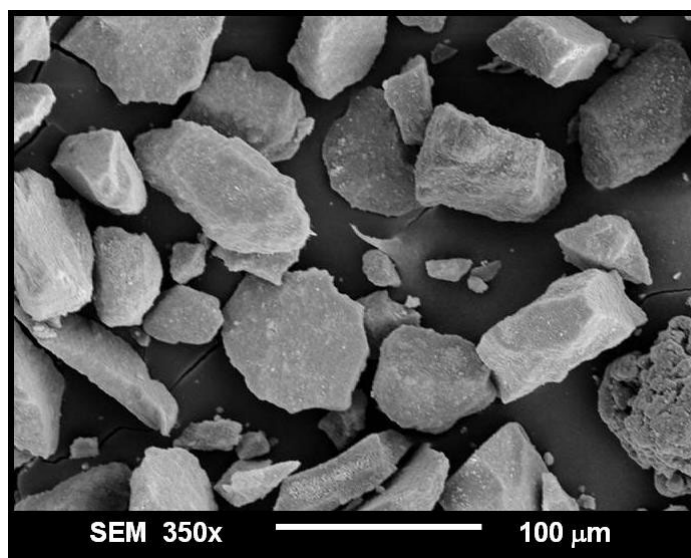
Figure 46. Precipitated iron F-T catalyst PPS3516-1 at TOS= 0 h (used in run SB-19102). Catalyst particles are irregularly shaped with sharp edges.
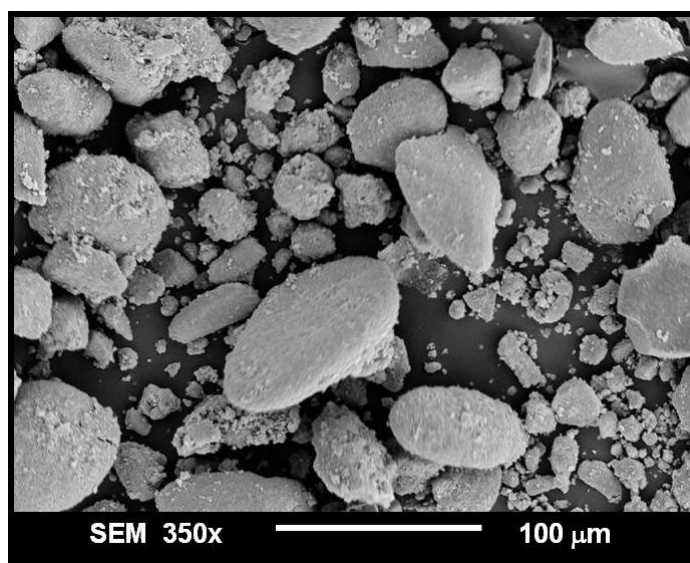
Figure 47. Precipitated iron F-T catalyst PPS3516-1 after 500 h in a STSR (run SB-19102). The number of small particles increased because of the attrition effect. Also the edges of larger particles are rounded due to erosion.
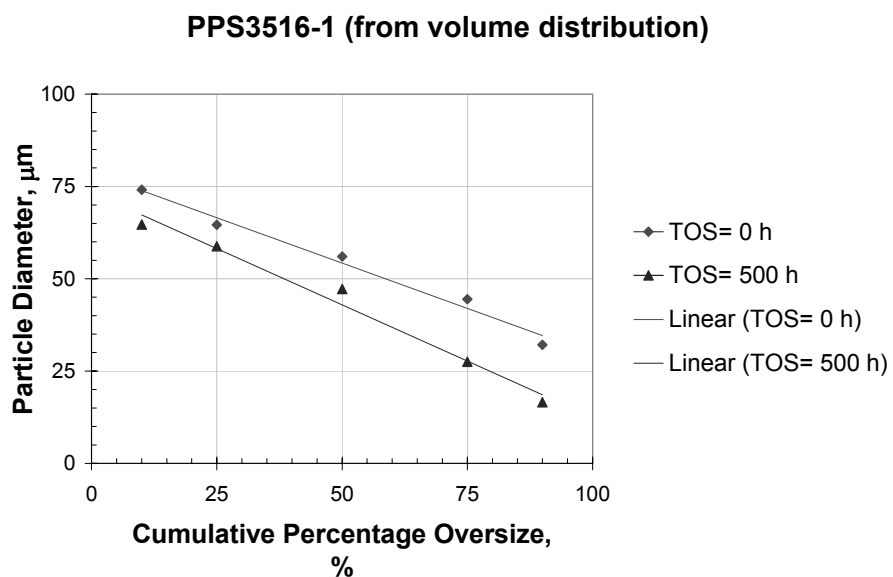
Figure 48. Percentiles (10, 25, 50, 75 and 90 %) obtained from volume distributions for the spray dried catalyst PPS3516-1 at TOS= 0 h and TOS= 500 h (run SB-19102).

Spray dried catalysts prepared from vacuum-dried precursors

A representative SEM micrograph of catalyst DPS5624-2 at TOS= 0 is given in Figure 49. This sample consists of particles larger than 50 μm and smaller particles of around 10 μm. Also some of the smaller particles (less than 10 μm) are attached together forming larger agglomerates which may be easy to break up during STSR testing. Figure 50 shows the same catalyst after 295 hours in the slurry reactor at 4-5.8 Nl/g-Fe/h, 260 ºC and 1.5-2.2 MPa (SB-16502). Attrition effect is obvious because of generation of small particles due to disintegration of agglomerates (fracture). This is also confirmed by PSD results shown in Figure 51. The Sauter mean diameter exhibited reduction by 31.5 %, whereas volume moment diameter was reduced by 18.6 % with respect to the catalyst sample collected at TOS= 0 h (Table 10).
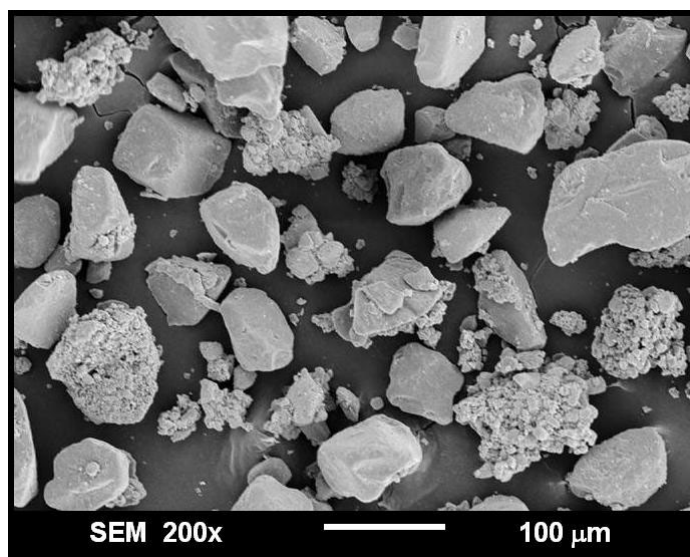
Figure 49. Spray dried catalyst DPS5624-2 prepared from dry precursors. SEM micrograph of withdrawn sample at TOS= 0 h (run SB-16502) shows the presence of large agglomerates formed of smaller particles (< 10 μm).
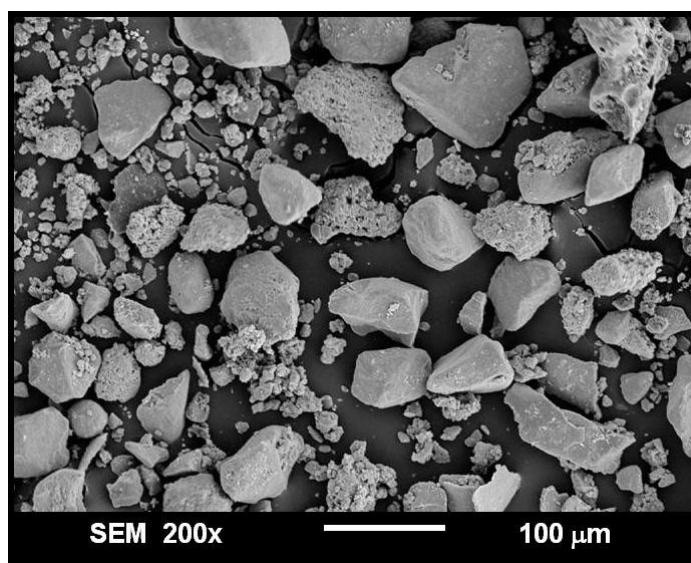
Figure 50. Spray dried catalyst DPS5624-2 prepared from dry precursors at TOS= 295 h. It can be observed that some large agglomerates disintegrated into small particles after the reaction test (run SB-16502).

DPS5624-2 (from volume distribution)
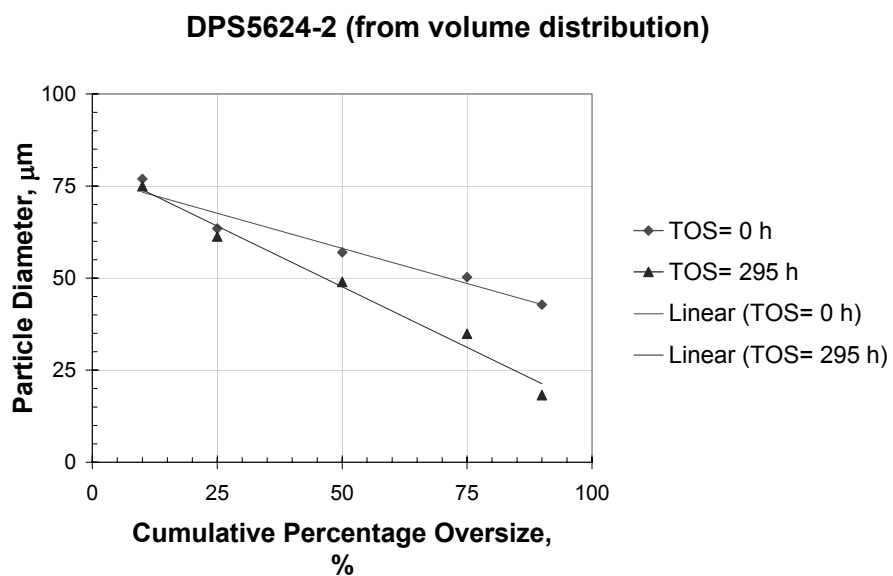
Figure 51. Percentiles (10, 25, 50, 75 and 90 %) obtained from volume distributions for the spray dried catalyst DPS5624-2 at TOS= 0 h and TOS= 295 h (used in run SB-16502).

Spray dried catalysts prepared from wet precursors

A representative SEM micrograph of catalyst WCS3516-1 (SiO_2 from colloidal silica) at TOS= 0 h is given in Figure 52. This sample consists of particles with excellent sphericity and smooth surface. Larger particles are around 30 μm in diameter, whereas smaller ones are around 5 μm in diameter. Figure 53 shows the same catalyst after 345 hours of testing at 4-6 Nl/g-Fe/h, 260 ºC and 1.5-2.4 MPa (SB-30702). From the SEM micrograph shown in Figure 53 it can be seen that this catalyst has a high attrition resistance, since its morphology practically remained unchanged. High attrition strength of this catalyst is also supported by particle size distribution results shown in Figure 54. Sauter mean diameter was reduced by 6.7 %, whereas the volume moment diameter was reduced by 5.6 % (Table 10).
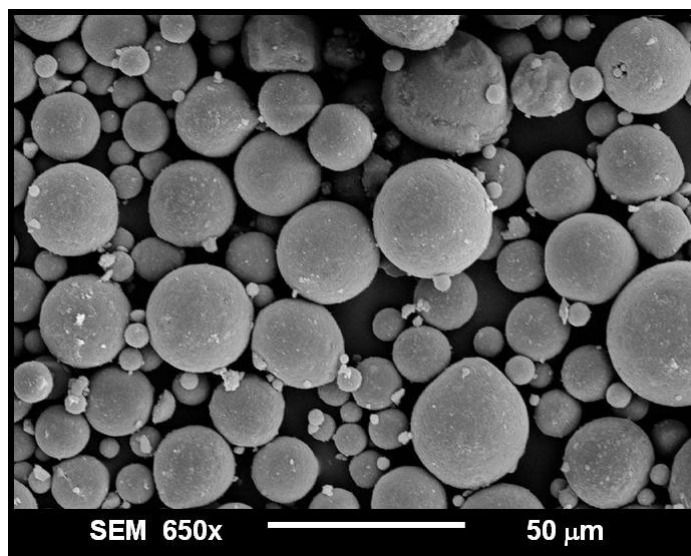
Figure 52. Spray dried catalyst WCS3516-1 prepared from wet precursor. SEM micrograph shows a sample withdrawn from the STSR (run SB-30702) at TOS= 0 h. Catalyst is formed of spherical particles with smooth surfaces.
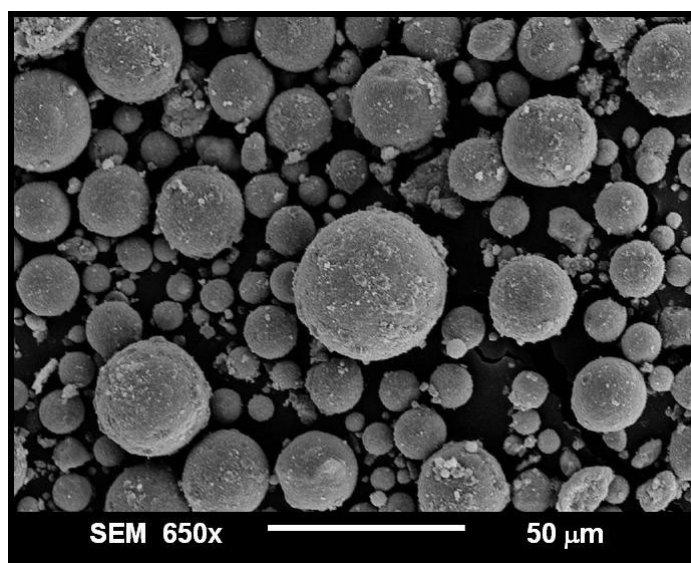
Figure 53. Spray dried catalyst WCS3516-1. SEM micrograph shows a sample withdrawn (run SB-30702) at TOS= 345 h. Catalyst morphology practically remained unchanged, except for a reduction in the smoothness of the catalyst's particles.
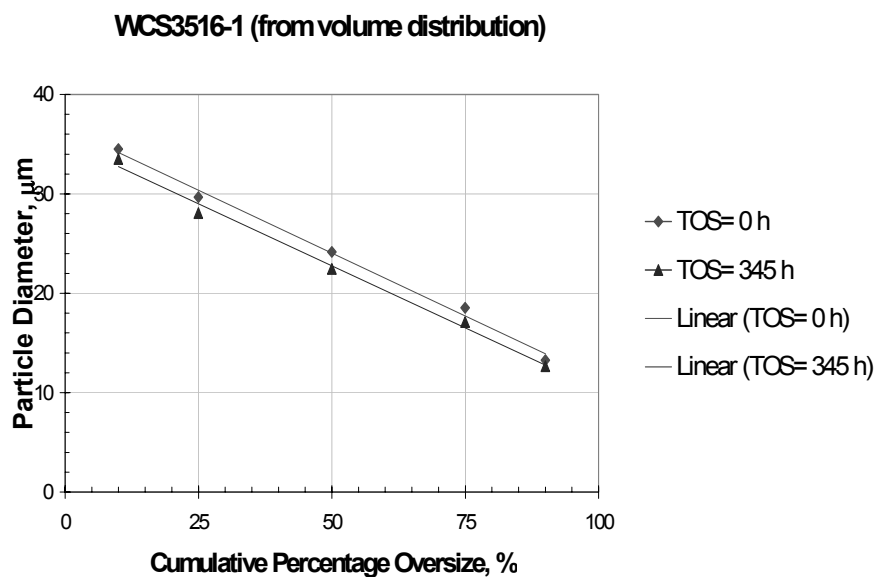
Figure 54. Percentiles (10, 25, 50, 75 and 90 %) obtained from volume distributions for the spray dried catalyst WCS3516-1 at TOS= 0 h and TOS= 345 h (Used in run SB-30702).

A SEM micrograph of catalyst WTO3516-1 withdrawn from the STSR (run SB-33802) at TOS= 0 h is shown in figures 55 and 56. Sample withdrawn at TOS= 0 h consists of spherical particles, but with cracks on their surfaces (Figure 55). A higher magnification (Figure 56) shows the presence of a significant number of particles smaller than 2 μm. The origin of these small particles may be due to particle disintegration which occurred during sieving and/or stirring in the STSR. SEM micrograph (Figure 57) of an as spray dried catalyst sample does not reveal presence of small particles. Figure 58 shows the same catalyst after 299 hours in the slurry reactor at 4-6 Nl/g-Fe/h, 260 ºC and 1.5-2.2 MPa (SB-33802). It is observed that practically all catalyst particles lost their sphericity after the reaction test. Formation of large agglomerates (~ 50 μm in diameter) might be due to incomplete removal of wax. Even though, this catalyst was washed two times using the same washing procedure that the one employed for catalyst WCS3516-1.
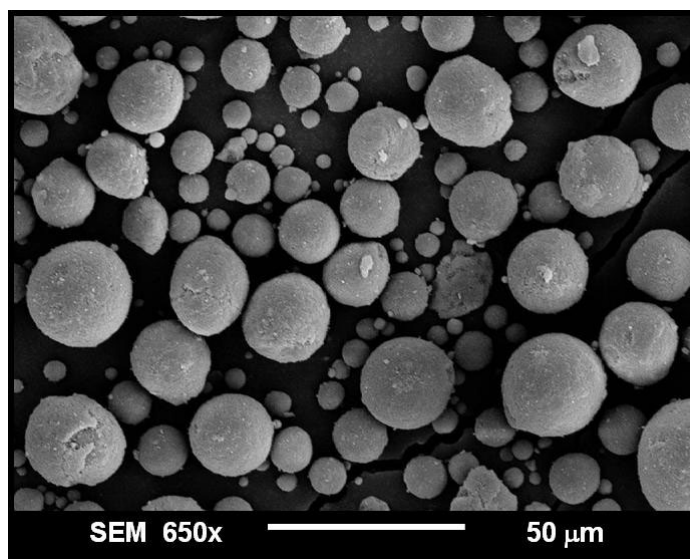
Figure 55. SEM micrograph of catalyst sample WTO3516-1 withdrawn from the STSR (run SB-33802) at TOS= 0 h. Most of the particles are spherical. However, some of them have irregularities and some particles are cracked, even at TOS= 0 h.
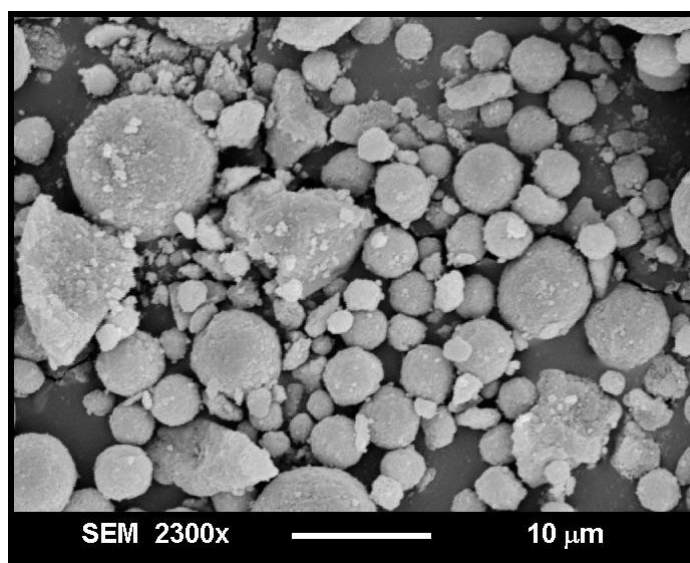
Figure 56. Higher magnification of WTO3516-1 catalyst withdrawn from the STSR (run SB-33802) at TOS= 0 h. There is evidence of particle disintegration during catalyst sieving and/or stirring in the STSR.
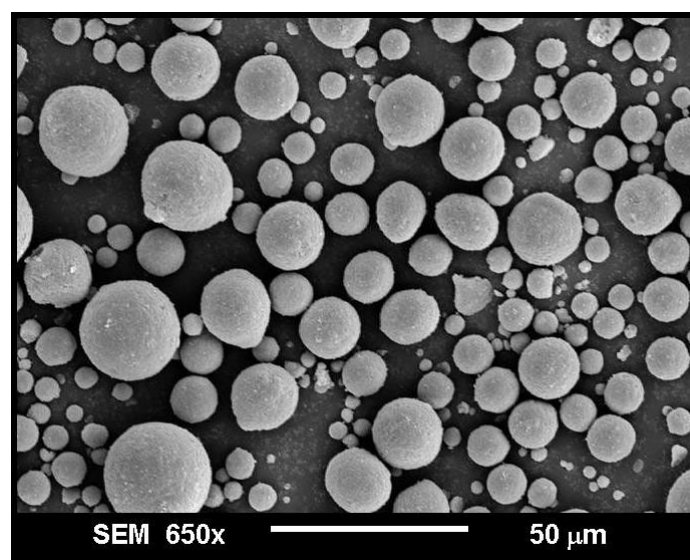
Figure 57. SEM micrograph of WTO3516-1 catalyst (as spray dried sample). Particles are mostly spherical with smooth surfaces.
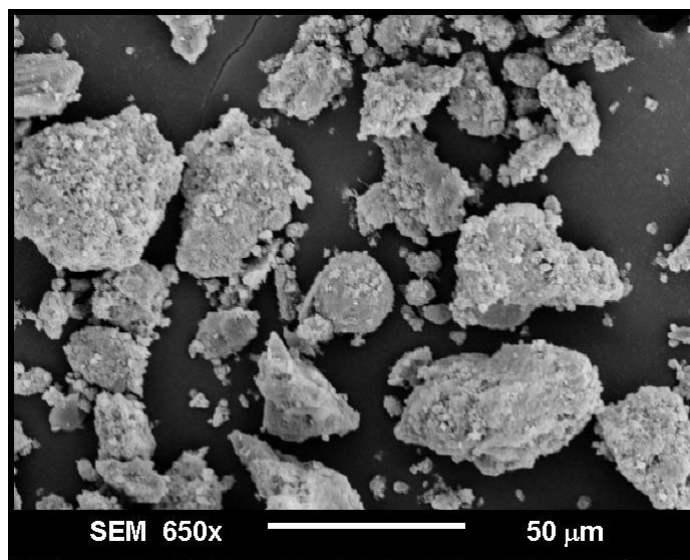
Figure 58. SEM micrograph of catalyst sample WTO3516-1 withdrawn from the STSR (run SB-33802) at TOS= 299 h. The sphericity of the particles disappeared after 299 h of testing in the STSR. Formation of large agglomerates was due to incomplete removal of wax.

From the PSD distribution for catalyst WTO3516-1 shown in Figure 59, it is obvious the formation of large agglomerates. From this figure it is observed that 10 % of the particles of sample collected at TOS= 0 h have a diameter larger than 25 μm, whereas for catalyst after 299 hours in the STSR, 10% of the particles have a diameter larger 62.5 μm due to particle agglomeration due to residual wax. Because of this, comparison of the attrition behavior of this catalyst with others will be limited to morphological comparisons.

WTO3516-1 (from volume distribution)
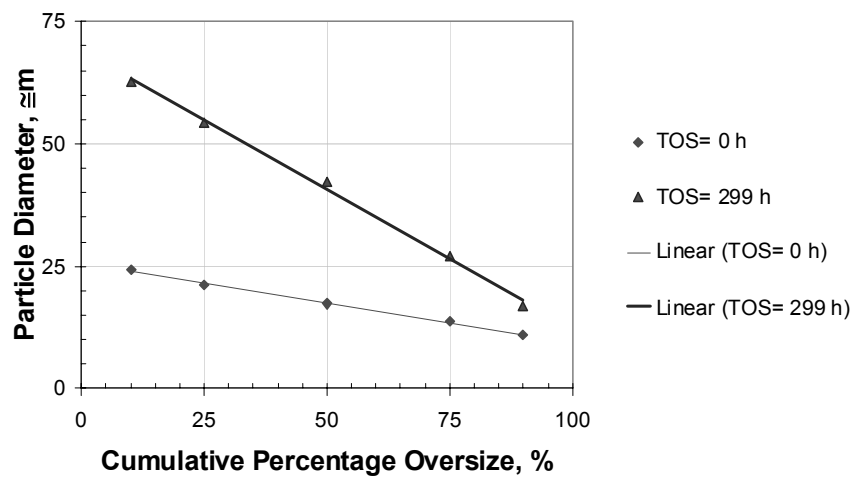
Figure 59. Percentiles (10, 25, 50, 75 and 90 %) obtained from volume distributions for the spray dried catalyst WTO3516-1 at TOS= 0 h and TOS= 299 h (Used in run SB-33802).

SUMMARY

Spray drying

Spray drying technique played an important role in this work. We started our experiments using model powders (iron oxide or iron oxide/Bindzil 30/360) in order to become familiar with the spray dryer operation. Subsequently, the observations derived from these experiments were used to define operational parameters for spray drying of iron catalyst from both vacuum-dried precursors and wet precursors. Some general observations from these experiments are given below.

Spray drying of model powders

Spray drying experiments, with iron oxide and iron oxide/Bindzil 30/360, in the APV Anhydro Lab. S1 spray dryer indicated that the morphology of spray-dried iron oxide was not markedly dependent upon operational parameters. All experiments with iron oxide powder showed that it did not agglomerate (Figures 21-23) regardless of conditions employed. However, addition of binder silica (Bindzil 30/360) lead to formation of either dimpled particles or spherical particles depending upon the operational parameters employed (i.e. feed properties). Observations derived from spray drying experiments with model powders were then used to define the operational parameters for spray drying of catalyst precursors.

Spray drying of catalysts from dry precursors

Catalysts DPS5624-2 and DPS3616 (see Table 8) were prepared from vacuum-dry precursors. Both catalysts were impregnated with potassium before spray drying. Additionally, silica binder (Bindzil 30/360) was added to catalyst precursor DPS3616 in slurry form (3 wt. % of catalyst total weight on dry basis). SEM micrographs of spray

dried catalysts (Figures 29 and 30) showed that they did not form spherical particles. Large particles were irregularly shaped, whereas smaller particles (~5 μm in diameter) were nearly spherical. Therefore, the attrition behavior of catalysts prepared by this method is expected to be similar to that of precipitated catalysts with similar composition and silica source.

Spray drying of catalysts from wet precursors

Catalysts series WPS3516, WCS3516 and WTO3516 (Nos. 8-10; 12; and 14-17 in table 8) where spray dried from wet precursors using potassium silicate, colloidal silica and TEOS as the silica source, respectively. All these catalysts, except WPS3516-1, formed spherical particles with smooth surfaces. Catalyst WPS3516-1 (Figure 31) consisted of dimpled particles due to the operation outside optimal parameters for spray drying step. It seems that formation of spherical particles is more dependent upon the operating conditions than on the source of silica. On the other hand, catalyst WTO3516-1 at TOS= 0 h showed the presence of cracks on the catalyst's surface (Figure 55), which were not observed in *as spray-dried* catalyst sample (Figure 57). Therefore, catalyst's sphericity does not necessarily imply high mechanical strength.

Spray-dried catalysts prepared at TAMU from wet precursors were more spherical than spray dried catalysts prepared at HU. However, TAMU's catalysts had a large fraction of particles smaller than 45 μm, regardless of operational conditions employed. In contrast, from sieving results with HU catalysts, it was observed that 16-39 wt. % of particles were larger than 45 μm (see Table 9). This is attributed to differences in spray drying equipment design and/or operating conditions employed.

Comparison of attrition behavior of iron F-T catalysts

Each catalyst exhibited different attrition behavior during STSR tests depending on its morphological and physical properties. It is expected that attrition results obtained from STSR tests will be useful to determine whether an iron F-T catalyst will be suitable for use in a SBCR. Physical attrition in a STSR is expected to be more severe than that in a SBCR.

Attrition behavior of catalysts tested in this work was evaluated on the basis of observed changes in morphological properties (via SEM), and changes in particle size distribution after STSR testing. In the latter case, PSD measurements were performed using the Coulter® Counter Multisizer. From PSD results, one can obtain several parameters which can be used to quantify attrition. These are: changes in Sauter mean diameter ($d_{3,2}$) and volume moment diameter ($d_{4,3}$), and change in fraction of fine particles (particles < 10 µm in diameter) during testing in the STSR. Sauter mean diameter was selected since this parameter is commonly used to represent the average particle size for applications in which the ratio to particle volume and surface area is important. On the other hand, the volume moment diameter was used previously in some of attrition studies of iron F-T catalysts [15-17, 26]. This parameter is biased towards large particles, since these particles occupy most of the catalyst volume. Finally, generation of fines is also important to asses attrition behavior of iron F-T catalysts, since fine particles cause separation problems during SBCRs' operation. Therefore, their quantification is an important issue in the assessment of the attrition behavior of iron F-T catalysts. Table 12 shows the percent of particles smaller than 10 and 20 µm in diameter before and after the reaction test for each catalyst used in the STSR. Generation of particles smaller than 20 µm in diameter has been selected, because in previous attrition studies of iron F-T catalysts ([15-17, 26]) this parameter was used to quantify the attrition strength. However, in this thesis we will emphasize the change in fraction of particles smaller than 10 µm in diameter, since small particles represent the major problem in catalyst/wax separation in SBCRs.

Table 12. Percent of particles below 10 and 20 μm in diameter before and after slurry reactor test (from volume distributions obtained using a Coulter® Counter Multisizer)

Catalyst ID	TOS= 0 h		*t**, h	TOS= *t* h		Change $	
	Fraction of particles, %			Fraction of particles, %		< 10 μm	< 20 μm
	< 10 μm	< 20 μm		< 10 μm	< 20 μm		
HU2061	0.4	2.0	380	62.9	70.9	62.5	68.9
HU1112	0.7	6.8	450	*7.4*	*12.1*	*6.7*	*5.3*
HU3471	0.5	10.3	449	*4.2*	*25.3*	*3.7*	*15.0*
CC3291	3.3	11.6	429	5.9	21.4	2.6	9.8
PPS3516-1	0.3	2.6	500	3.0	14.9	2.7	12.3
DPS5624-2	1.0	2.0	295	3.3	11.6	2.3	9.6
WCS3516-1	4.1	32.2	345	4.8	41.1	0.7	8.9
WTO3516-1	7.0	69.0	299	*3.6*	*14.2*	*-3.4*	*-54.8*

* Time of exposure.
$ Change = ($W_{@TOS=t\,h}$ − $W_{@TOS=0\,h}$); where W= percent of particles < 10 or 20 μm.
Italics are used when samples were washed several times.

Spray-dried catalysts prepared at HU

Three spray-dried catalysts prepared at HU were tested in the STSR for 380-450 hours (Table 10). Catalysts HU2061 and HU1112 contain 11 and 16 parts of precipitated silica (from TEOS), respectively, whereas catalyst HU3471 contains 1.1 parts of silica binder per 100 parts of Fe. Morphological analyses of catalysts samples collected at TOS= 0 h show that catalyst HU2061 has a large number of platelet-like particles (Figure 34), whereas catalysts HU1112 and HU3471 have quite similar morphologies (Figures 40 and 37). These two catalysts have a large number of spherical particles with rough surfaces. After testing in the STSR for 380-450 hours, their morphologies changed. Catalyst HU2061 disintegrated into a significant number of small pieces due to fracture effects (Figure 35). Both HU1112 and HU3471 catalysts lost their sphericity after ~450 hours in the STSR (Figures 41 and 38). However, the generation of fines was relatively small. This may be caused, to some extent, by multiple washings to remove residual wax. It is possible that some fines were lost during washing procedure. The attrition results obtained from PSD measurements (Table 13) showed that catalysts HU1112 and HU3471 had similar reduction in their Sauter mean diameters (32.7 and 39.9 %, respectively) after testing in the STSR. Change in fraction of fine particles (diameter less

than 10 μm) for these two catalysts was also similar (6.7 and 3.7 %, respectively). On the other hand, the change in volume moment diameter for these two catalysts showed an unexpected behavior. The volume moment diameter of HU1112 catalyst decreased by 5.7 % only (Table 13), whereas that of HU3471 catalyst increased by 2.2 % (listed as -2.2 % in Table 13). This behavior (increase in particle size) was not evident from SEM micrographs (Figures 38 and 41).

Table 13. Summary of PSD results obtained using the Coulter® Counter Multisizer (from volume distributions)

Catalyst ID	SiO_2 content	Run #	t^*, h	% Change after t hours in the STSR		Change in fraction of fines	
				$\Delta d_{3,2}$	$\Delta d_{4,3}$	$< 10\ \mu m$	$< 20\ \mu m$
HU2061	11 (P)	SB-20601	380	87.0	65.7	62.5	68.9
HU1112	16 (P)	SB-11102	450	32.7	5.6	6.7	5.3
HU3471	1.1 (B)	SB-34701	449	39.9	-2.2	3.7	15.0
CC3291	25 (P)	SB-32901	429	24.3	14.3	2.6	9.8
PPS3516-1	16 (P)	SB-19102	500	34.6	18.6	2.7	12.3
DPS5624-2	24 (P)	SB-16502	295	31.5	16.1	2.3	9.6
WCS3516-1	16 (B)	SB-30702	345	6.8	5.4	0.7	8.9
WTO3516-1	16 (P)	SB-33802	299	-85.9	-135.6	-3.4	-54.8

[*] Time of exposure; (P) precipitated silica; (B) binder silica.

As stated above, the volume moment diameter has bias towards large particles. Therefore, the increase in the volume moment diameter of catalyst HU3471, and small reduction observed with catalyst HU1112 may be caused by agglomeration of particles due to residual wax, and loss of small particles during washing procedure to obtain wax-free catalyst samples. In spite of unusual results for the volume moment diameter, the similarities in the attrition behavior of HU1112 and HU3471 catalysts are evident.

Attrition results (Table 13) show that HU2061 catalyst had much lower attrition resistance relative to catalysts HU1112 and HU3471. This catalyst experienced large changes in Sauter mean and volume moment diameters (85 and 65.7 %, respectively)

after 380 h of testing in the STSR. The inferior attrition strength of this catalyst is also reflected in considerable generation of particles < 10 mm in diameter during the STSR test (62.5 %)..

It can be concluded that mechanical integrity of catalysts HU2061, HU1112 and HU3471 was markedly dependent upon their morphological features. The attrition strength of catalysts made out of largely spherical particles was considerably higher than that of the catalyst consisting of irregularly shaped particles (i.e. platelet-like particles).

Spray-dried catalysts prepared from dry-precursors and precipitated catalysts

Two precipitated catalysts (PPS3516-1 and Ruhrchemie catalyst - CC3291) containing 16 and 25 parts of silica, respectively, and a spray-dried catalyst prepared from a vacuum-dried precursor (DPS5624-2 containing 24 parts of precipitated silica) were tested in the STSR for 500, 429 and 295 hours, respectively. SEM micrographs (Figures 46 and 44) of precipitated catalysts (PPS3516-1 and CC3291) at TOS= 0 h show that they are formed of irregularly shaped particles with sharp edges and smooth surfaces. After testing in the STSR the Ruhrchemie catalyst's morphology did not change much (Figures 44 and 45). At the end of the test, the catalyst had slightly smoother edges and surfaces. A similar behavior was observed with catalyst PPS3516-1, but the attrition effect was more markedly pronounced. After 500 hours in the STSR, the catalyst's particles had smoother surfaces with markedly rounded edges due to the erosion effect (Figure 47). On the other hand, catalyst DPS5624-2 collected at TOS= 0 h (Figure 49) was formed of large irregularly shaped particles, whereas smaller particles (<5 μm) were nearly spherical. Figure 50 shows this catalyst after 295 hours in the STSR, and morphological changes of this catalyst are similar attrition to those observed with precipitated catalysts. However, the fracture effect was slightly greater compared to the Ruhrchemie catalyst.

The attrition results obtained from PSD measurements (Table 13) show that precipitated catalysts CC3291 and PPS3516-1 have similar mechanical strength, as spray-dried catalyst DPS5624-2 prepared from the vacuum-dry precursor. Changes in the volume moment and Sauter mean diameters for these three catalysts were 24.3-34.6 % and 14.3-18.6 %, respectively. Both, change in the volume moment diameter and Sauter mean diameter indicate that Ruhrchemie catalyst (CC3291) was more attrition resistant compared to catalysts PPS3516-1 and DPS5624-2.

Changes in fraction of particles smaller than 10 μm in diameter, after 295-500 hours in the STSR (Table 13), also demonstrated similarities in the attrition behavior of these three catalysts. Therefore, from PSD results it can be concluded that spray drying of the vacuum-dry precursor did not result in improvement of the attrition strength relative to precipitated iron catalysts, which were not spray dried. This is consistent with SEM results, which showed that the spray-dried catalyst had similar morphology as the two precipitated catalysts.

Spray-dried catalysts prepared from wet form. Colloidal silica vs. TEOS as the silica source

Catalysts WCS3516-1 and WTO3516-1 were spray dried from wet slurries having the same composition (100 Fe/3 Cu/5 K/16 SiO_2), but were prepared using different silica sources. Catalyst WCS3516-1 was prepared using colloidal silica as the silica source, whereas catalyst WTO3516-1 was prepared using TEOS. Both catalysts were impregnated with potassium by I.W.I. method after spray drying.

SEM micrographs of catalyst samples at TOS= 0 h (Figures 52 and 55) show that both catalyst are formed of mostly spherical particles. However, catalyst WTO3516-1 showed the presence of cracks and some irregularities on the surface of the catalyst's particles, which might have an adverse effect on attrition resistance of this catalyst. After 299 h of testing in the STSR WTO3516-1 catalyst lost its sphericity due to attrition effects

(Figure 58). Also, formation of large agglomerates was observed after the reaction test. In contrast, WCS3516-1 catalyst had an excellent attrition resistance. After 345 hours of testing in the STSR the catalyst's morphology remained practically unchanged relative to catalysts sample at TOS= 0 h (Figures 53 and 52, respectively).

Results from PSD measurements with catalyst WCS3516-1 confirmed its excellent attrition resistance. Reductions in the volume moment and Sauter mean diameters (5.4 and 6.8 %, respectively) were the smallest among all catalysts used in this work. Small increase in the fraction of particles smaller than 10 μm in diameter (Table 13) indicates that this catalyst did not experience significant attrition by erosion, which makes this catalyst suitable for use in SBCRs.

PSD results from the STSR test of WTO3516-1 catalyst (Figure 59 and Table 12) show increase in the average particle size. This phenomenon is attributed to the presence of residual wax. However, it is not clear why this catalyst, as well as catalysts HU1112 and HU3471, had this problem. They were washed several times using the same procedure than was employed with other catalysts. In spite of the absence of reliable results from PSD measurements, it is clear from SEM images that the spray-dried catalyst prepared with colloidal silica is more attrition resistant than the catalyst prepared using TEOS as the silica source.

Attrition behavior. Overall assessment

From SEM micrographs and PSD results the following conclusions can be derived:

- Catalyst WCS3516-1 containing 16 parts of silica from colloidal silica had the highest attrition strength among all catalysts tested.

- On the opposite extreme was catalyst HU2061 containing 11 parts of silica from precipitated TEOS. Poor attrition resistance of this catalyst illustrates the

importance of choosing the proper spray-drying parameters. This catalyst was in the form of platelet-like particles, which broke up easily into smaller particles during the STSR test.

+ Ruhrchemie (CC3291) and precipitated PPS3516-1 catalysts exhibited comparable or superior attrition resistance relative to spray-dried catalysts prepared at HU (HU3471 and HU1112). This shows that spherical (or nearly spherical) morphology of spray-dried catalysts does not imply superior attrition strength relative to that of irregularly shaped precipitated iron catalysts. Physical properties (porosity and particle density) of catalyst particles also have significant effect on attrition resistance.

+ Ruhrchemie (CC3291) catalyst and DPS5624-2 catalyst (spray-dried from the dry precursor) exhibited similar attrition behaviors. It can be concluded that spray drying of dry precursors (after vacuum drying) did not impart any additional strength to dry precursors, at least not under parameters selected in this work for the spray drying step and preparation of slurry feed.

+ As mentioned throughout this work, generation of fines, especially particles smaller than 10 μm in diameter, is the main problem in SBCRs' operation. Since generation of fine particles was small with all catalysts tested (except for HU2061 catalyst), it may be concluded that these catalysts are good candidates for use in slurry bubble column reactors for F-T synthesis.

REFERENCES

[1]   B.H. Davis, Catal. Today 71 (2002) 249.

[2]   M.E. Dry in: J.R. Anderson, M. Boudart (Eds.), Catalysis Science and Technology, Vol. 1, Springer, New York, 1981, p.160.

[3]   A. Geertsema, Indirect Liquefaction Contractors Review Meeting Proceedings, (1990) p. 273.

[4]   A. Geertsema, Plenary paper presented at the 10th Pittsburgh Coal Conference Pennsylvania, 24 September 1993.

[5]   B. Jager and R. Espinoza, Catal. Today, 23 (1995) 17.

[6]   B. Jager, Stud. Surf. Sci. Catal., 107 (1997) 219.

[7]   C. Hill, Sasol's Experience in the Conversion of Gas into Liquids, Retrieved November 7-8, 1999, from: http://www.iies.org/english/training-conf/conference/conf99-paper/pdf/Cavan%20hill.pdf

[8]   B. Bukur, C. Sivaraj, Appl. Catal. A: Gen. 231 (2002) 201.

[9]   H. Kölbel, M. Ralek, Catal. Rev. Sci. Eng. 21 (1980) 225.

[10] S. Kalakkad, M.D. Shroff, S. Kohler, N. Jackson and A.K. Datye, Appl. Catal. 133 (1995) 335.

[11] A.K. Datye, M.D. Shroff, Y. Jin, R.P. Brooks, M.S. Harrington, A.G. Sault and N.B. Jackson, Stud. Surf. Sci. Catal. 101 (1996) 1421.

[12] H.N. Pham, J. Reardon and A. K. Datye, Power Tech., 103 (1999) 95

[13] H.N. Pham, A. Viergutz, R.J. Gormley, A.K. Datye, Powder Tech. 110 (2000) 196.

[14] H. N. Pham, A. K. Datye, Cat. Today 58 (2000) 223.

[15] J.G. Goodwin Jr., K. Jothimurugesan, S.K. Gangwal, J.J. Spivey, Catal. Today 58 (2000) 335.

[16] K. Sudsakorn, J. G. Goodwin Jr., K. Jothimurugesan, A. A. Adeyiga, Ind. Eng. Chem. Res. 40 (2001) 4778.

[17] K. Jothimurugesan, J.J. Spivey, S.K. Gangwal, and J.G. Goodwin Jr., in: "Natural Gas Conversion V", Stud. Surf. Sci. Catal., 119, (1998) 215.

[18] ASTM D5757-95, Standard Test Method for Determination of Attrition and Abrasion of Powdered Catalysts by Air Jets, American Society for Testing and Materials, 1995.

[19] D.B. Bukur, S.A. Patel, X.S. Lang, Appl. Cat. 61 (1990) 329.

[20] D.B. Bukur, L. Nowicki, X.S. Lang, Chem. Eng. Sci. 49 (1994) 4615.

[21] D. B. Bukur, X.S. Lang, Ind. Eng. Chem. Res. 38 (1999) 3270.

[22] J.C.W. Kuo, Final Report Prepared for DOE, Contract no. DE-AC22-83PC600019, Mobil Research and Development Corp., Paulsboro, NJ, 1985.

[23] H. Kölbel, P. Ackerman, F. Engelhardt, in: Proceedings of the 4th World Petroleum Congress Section IV/C, Carlo Colombo Publishers, Rome, 1955, 9. 227.

[24] E. Ortega Rivas, Food Powder Processing in: UNESCO Encyclopedia of Life Support Systems, EOLSS Publishers Co. Ltd., Oxford, UK, 2001.

[25] C.R. Bemrose, J. Bridgwater, Powder Tech. 49 (1987) 97.

[26] R. Zhao, K. Sudsakorn, J. G. Goodwin Jr., K. Jothimurugesan, S. K. Gangwal, J. Spivey, Catal. Today 71 (2002) 319.

[27] D. Wei, J.G. Goodwin Jr., R. Oukaci, A. H. Singleton, Appl. Cat. A: Gen. 210 (2001) 137.

[28] R. Zhao, J.G. Goodwin Jr., R. Oukaci, Appl. Cat. A: Gen. 189 (1999) 99.

[29] S.A. Weeks, P. Dumbill 1990, Oil and Gas J., 88 (1990) 38.

[30] R. Zhao, J.G. Goodwin Jr., K. Jothimurugesan, J.J Spivey, S.K. Gangwal, Ind. Eng. Chem. Res., 39 (2000), 1155.

[31] W.L. Forstyle Jr., W.R. Hertwig, Ind. Eng. Chem., 41 (1949) 1200.

[32] J.E. Gwyn in: On the Particle Size Distribution Function and the Attrition of Cracking Catalysts, AIChe Symposium Series, Vol. 15, American Institute of Chemical Engineers, New York, 1969, p 35.

[33] J. Werther, W. Xi, Powder Tech., 76 (1993) 39.

[34] S.G. Thoma, M. Ciftcioglu, D.M. Smith, Powder Tech., 68 (1991) 53.

[35] K. Masters, in: Spray Drying Handbook, Fifth edition, Longman Scientific and Technical (Ed.), Denmark, 1991.

[36] D.E. Walton, Drying. Tech., 18 (2000) 1943.

[37] T. Allen, in: Particle Size Measurement, Forth edition, Powder Technology Series, Chapman and Hall, New York, 1990, p. 455.

[38] R. H. Berg, in: Symposium on Particle Size Distribution, ASTM Publication No. 234, American Society for Testing and Materials, 1958.

[39] K. R. Schrag and M. Corn, Am. Ind. Hyg. Assoc. J., July/August, 1970, 446.

[40] J. Simecek, Staub Reinhalt Luft, 27 (1967) 33.

[41] C.D. Frohning, W. Rotting, F. Schnur, in: The Fixed Bed Synthesis, J. Falbe (Ed.), Stuttgart, Germany, 1977, p. 234.

[42] D. B. Bukur, X.S. Lang, D. Mukesh, W.H. Zimmerman, M.P. Rosynek and C. Li, Ind. Eng. Chem. Res. 28 (1989) 1130.

[43] D.B. Bukur, S.A. Patel, X.S. Lang, Appl. Cat. 61, (1990) 329.

[44] D.B. Bukur, L. Nowicki, X.S. Lang, Chem. Eng. Sci. 49 (1994) 4615.

[45] D. Bridges, J. Brady, B. Newton, Scanning Electron Microscopy and X-Ray Microanalysis, 2000, retrieved from: http://www.science.smith.edu/departments/ SEM/ Manual99.pdf

VITA

Name:	Víctor Hugo Carreto Vázquez
Address:	Gardenia No. 206, Col. Las Flores, Cd. Netzahualcoyotl
	Estado de México, C. P. 57310, México
Educational background:	B.S. Industrial Chemical Engineering
	Chemical Engineering
	E.S.I.Q.I.E.-I.P.N.
	1994-1999.